field, and Walters.[2] Figure 6 shows the measured electron densities vs 2^3S_1 density (a quantitative measure of the intensity of the discharge) for He^4 sample pressures of 0.1 and 0.22 torr. Under sample conditions closely approximating those employed and analyzed by McCusker *et al.* (8% absorption of He^4 pumping light on He^4 sample and pressure of 0.1 torr) in extracting an optimum polarized electron beam, the electron density is approximately 7×10^7 cm^{-3}. However, the error could be as large as a factor of 2, primarily because of uncertainty in the proportionality constant k in Eq. (14), taken here to be 230 $cm^3\,sec^{-1}$ appropriate to a uniform electron distribution.

†Based on a Master of Arts thesis by J. C. Hill (Rice University, 1969). Work supported in part by U. S. Atomic Energy Commission.

*Present address: Physics Department, Duquesne University, Pittsburgh, Pa. 15219.

‡Present address: Physics Department, Texas Tech University, Lubbock, Tex. 79409.

§Present address: Aerospace Corporation, San Bernadino, Calif. 92401.

[1]C. C. Lin and R. G. Fowler, Ann. Phys. (N. Y.) 15, 461 (1961).

[2]M. V. McCusker, L. L. Hatfield, and G. K. Walters, preceding paper, Phys. Rev. A 5, 177 (1972). See also M. V. McCusker, L. L. Hatfield, and G. K. Walters, Phys. Rev. Letters 22, 817 (1969).

[3]M. A. Biondi, Phys. Rev. 88, 660 (1952).

[4]A. V. Phelps, Phys. Rev. 99, 1307 (1955).

[5]A. V. Phelps and J. P. Molnar, Phys. Rev. 89, 1202 (1953).

[6]D. D. McCracken and W. S. Dorn, *Numerical Methods and Fortran Programming* (Wiley, New York, 1964), p. 317.

[7]A. C. G. Mitchell and M. W. Zemansky, *Resonance Radiation and Excited Atoms* (Cambridge U.P., Cambridge, England, 1961), Chap. 3.

[8]J. C. Ingraham and S. C. Brown, Phys. Rev. 138, A1015 (1965).

[9]S. C. Brown, *Introduction in Electrical Discharges in Gases* (Wiley, New York, 1966), p. 61.

[10]F. D. Colegrove and P. A. Franken, Phys. Rev. 119, 680 (1960).

[11]L. D. Schearer, *Advances in Quantum Electronics* (Columbia U.P., New York, 1961), pp. 239–251.

[12]F. D. Colegrove, L. D. Schearer, and G. K. Walters, Phys. Rev. 132, 2561 (1963).

[13]R. C. Greenhow, Phys. Rev. 136, A660 (1964).

[14]This relation holds only for $P \ll 1$, a condition satisfied in the present experiment.

[15]H. J. Oskam, Philips Res. Rept. 13, 335 (1958).

[16]W. A. Fitzsimmons, L. L. Tankersley, and G. K. Walters, Phys. Rev. 179, 156 (1969).

[17]L. A. Weaver and R. J. Freiberg, J. Appl. Phys. 39, 4283 (1968).

PHYSICAL REVIEW A VOLUME 5, NUMBER 1 JANUARY 1972

Polarized Electrons from Photoionization of Polarized Alkali Atoms*

V. W. Hughes, R. L. Long, Jr.,† M. S. Lubell, M. Posner,‡ and W. Raith
Yale University, New Haven, Connecticut 06520
(Received 30 June 1971)

The process of photoionization of polarized alkali atoms in an atomic beam has been studied for potassium and lithium. Depolarization processes associated with photoionization of alkali molecules and optically excited atoms were discovered. After eliminating these depolarization mechanisms, the measured photoelectron polarization agreed within an accuracy of 3% with the predicted polarization based on the current theory for this electric dipole process. Using a polarized Li^6 atomic beam and a pulsed uv light source, we have produced an intense and highly polarized electron beam with 2×10^8 electrons in 1.5 μsec and with a polarization of 0.78, which is a suitable prototype injector source for a high-energy electron accelerator.

I. INTRODUCTION

Investigation of the spin polarization of electrons from atomic systems is a valuable approach to the study of basic atomic processes. In addition, such investigation provides a basis for the development of a source of polarized electrons. One of the earliest proposals for producing polarized electrons was made in 1930 by Fues and Hellman,[1] who suggested that polarized electrons could be obtained from photoionization of a polarized alkali-atom beam. The suggestion was based upon the fact that photoionization is primarily an electric dipole transition, and hence the ejected photoelectrons should have the same polarization as the valence electrons of the alkali atoms. The first attempt to study this process was made in 1961 by Friedmann, who reported obtaining an electron beam of high intensity and high polarization.[2] Friedmann's results, however, could not be reproduced.[3,4]

Our work at Yale was begun with two objectives —the study of the spin-dependent effects in the photoionization of alkali atoms, and the development of a polarized electron source which would be use-

ful in other experiments in atomic, nuclear, and particle physics. During the course of our work we discovered and analyzed several depolarization mechanisms. Photoionization of alkali molecules and of optically excited atoms were studied and eliminated, and the implications of the recently discovered spin-orbit perturbation in the continuum P states[5-7] were evaluated. Our measurements of the spin polarization of photoelectrons from polarized potassium atoms[8] provided the first verification of the long-standing proposal of Fues and Hellman. Subsequent work on photoionization of polarized Li^6 atoms yielded results of increased accuracy showing that the polarization of the photoelectrons does agree very well with the theoretical expectation.

We then investigated pulsed photoionization of lithium employing a spark light source and developed a pulsed source of highly polarized electrons with high intensity. This source is suitable for atomic physics experiments on the spin dependence of electron interactions and also as an accelerator injector source for experiments at high energies.[9] Spin-dependent electron interactions are of great current interest in atomic[10-12] and particle physics.[13-19]

The present paper gives a detailed account of our experiments on the photoionization of polarized alkali atoms. Section II presents a brief description of the relevant theory; Sec. III describes the apparatus and experimental procedure; Sec. IV contains the results of the experiments on potassium and lithium photoionization, as well as a comparison of polarized electron sources based on the different available methods. Brief reports of this research have already been published.[3,8,9,20-24]

II. THEORY OF EXPERIMENT

A. Definitions

The polarization vector for a beam of electrons is defined as the expectation value of the Pauli spin operator,[25]

$$\vec{P} = \langle \vec{\sigma} \rangle = \mathrm{Tr}(\rho \vec{\sigma}) , \tag{2.1}$$

where ρ is the density matrix.[26] For relativistic electron beams, the polarization is given for the rest frame of the electrons. The direction of the beam is used as reference for the direction of $\vec{P}$, with the most important cases being longitudinal and transverse polarization.

In interactions which are polarization dependent, the observable signal I can be expressed as

$$I = I_0 (1 + \vec{P} \cdot \vec{A}) , \tag{2.2}$$

where I_0 is the signal obtained with unpolarized incident electrons and $\vec{A}$ is the analyzing power which describes the polarization dependence of the interaction. The product $|\vec{P}||\vec{A}|$ is customarily called the polarization asymmetry δ.

B. Polarized Atoms

Alkali atoms with a net electronic polarization are obtained through state selection by magnetic deflection in the inhomogeneous field of a six-pole magnet. The relevant part of the Hamiltonian for an alkali atom in its $^2S_{1/2}$ ground state is given by

$$\mathcal{H} = a \vec{I} \cdot \vec{J} + \mu_B g_I \vec{I} \cdot \vec{H}_0 + \mu_B g_J \vec{J} \cdot \vec{H}_0 , \tag{2.3}$$

in which a is the hyperfine-structure (hfs) interaction constant, I is the nuclear spin, J is the electronic angular momentum ($J = S = \frac{1}{2}$ for the alkali ground state), μ_B is the Bohr magneton, g_I and g_J are the nuclear and electronic g values, respectively, and H_0 is the external magnetic field.[27] The energy eigenvalues are given by the Breit-Rabi formula,

$$W_{F=I\pm 1/2,\, m} = -\frac{\Delta W}{2(2I+1)} + \mu_B g_I H_0 m \pm \frac{\Delta W}{2}\left(1 + \frac{4mx}{2I+1} + x^2\right)^{1/2} , \tag{2.4}$$

in which W is the energy of the terms specified by the total angular momentum quantum number $F = I \pm J$ (with $J = \frac{1}{2}$) and the magnetic quantum number m, ΔW is the zero-field hfs separation between the states $F = J + \frac{1}{2}$ and $F = J - \frac{1}{2}$, and

$$x = (g_J - g_I)\, \mu_B H_0 / \Delta W . \tag{2.5}$$

If the z axis is taken as the direction of the external magnetic field H_0, the magnetic moment of the atom in a state designated by the low-field quantum numbers F and m has a component along the field direction

$$\mu_z = -\frac{\partial W(F, m)}{\partial H_0} . \tag{2.6}$$

The energy eigenvalues and magnetic moments of the Zeeman states of a ground-state alkali atom with nuclear spin $I = 1$ (e.g., Li^6) are shown as functions of the magnetic field in Fig. 1.

The six-pole magnet produces the atom state selection in the strong-field region of the magnet gap. Atoms with the electronic magnetic quantum number $m_J = +\frac{1}{2}$ are transmitted preferentially. After leaving the six-pole magnet, the atoms enter a region where the photoionization takes place and where the magnetic field H is longitudinal (along the z axis). Since the transition from the six-pole field to the field of the ionization region is adiabatic, the electronic polarization of the transmitted atoms can be written as

$$P_{e,\,\mathrm{atom}} = \langle \sigma_z \rangle = s f(H) . \tag{2.7}$$

The quantity s is the state-selection parameter describing the effectiveness of the six-pole magnet

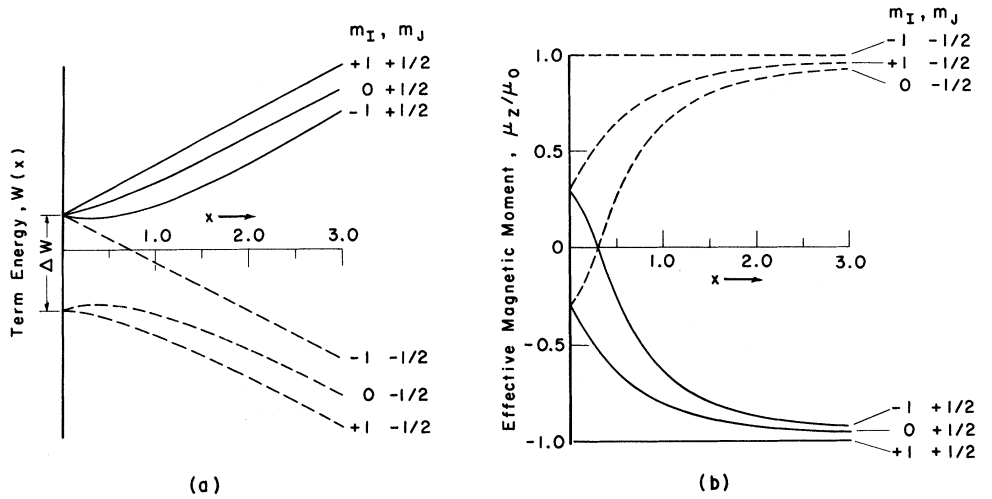

FIG. 1. Breit-Rabi diagram and plot of the effective magnetic moments for a $^2S_{1/2}$ atom with nuclear spin $I=1$. A perfect high-field state separation leads to the elimination of the terms represented by dashed curves.

(cf. Sec. III A) and is given by

$$s=(N^+-N^-)/(N^++N^-)\,, \tag{2.8}$$

in which N^+ and N^- are the number of transmitted atoms in states with $m_J=+\frac{1}{2}$ and $-\frac{1}{2}$, respectively. The state-selected atomic beam can be considered as a superposition of two beam components with weights of $(1-s)$ and s respectively, the former not being state selected and the latter containing only atoms with $m_J=+\frac{1}{2}$. The unselected component has zero electronic polarization at any field; the other component has an electronic polarization given by the function $f(H)$. In order to calculate this function, we assume that to a good approximation the magnetic state selection depends only on the strong-field magnetic quantum number m_J and that, therefore, the preferentially transmitted states with $m_J=+\frac{1}{2}$ and $m_I=I,\ (I-1),\ldots,\ -I$ are all equally populated. Since the nuclear magnetic moment is very small compared with the electronic spin magnetic moment, one can use the approximations

$$g_J-g_I\simeq g_J\simeq 2 \quad\text{and}\quad \langle\sigma_z\rangle\simeq-\mu_z/\mu_B\,. \tag{2.9}$$

By taking the average of the electronic polarization for the group of states with $m_J=+\frac{1}{2}$ (those represented by solid lines in Fig. 1), one finds

$$f(H)=\frac{1}{(2I+1)}\sum_{m=-I+1/2}^{I+1/2}\langle I+\tfrac{1}{2},m\,|\,\sigma_z\,|\,I+\tfrac{1}{2},m\rangle\,, \tag{2.10}$$

where

$$\langle I+\tfrac{1}{2},m\,|\,\sigma_z\,|\,I+\tfrac{1}{2},m\rangle=\frac{2m/(2I+1)+x}{\{1+[4m/(2I+1)]x+x^2\}^{1/2}} \tag{2.11}$$

as seen from Eqs. (2.9), (2.6), and (2.4). The function $f(H)$ is plotted in Fig. 2 for the two atoms Li^6 and K^{39}. Note that in a strong field H where electronic and nuclear spins are decoupled the function $f(H)$ approaches unity.

Table I presents data which are relevant for high-field state separation of one-electron atoms.[27,28] The values of $\Delta W/\mu_B$ in the last column correspond to $x=2$ in the Breit-Rabi equation and

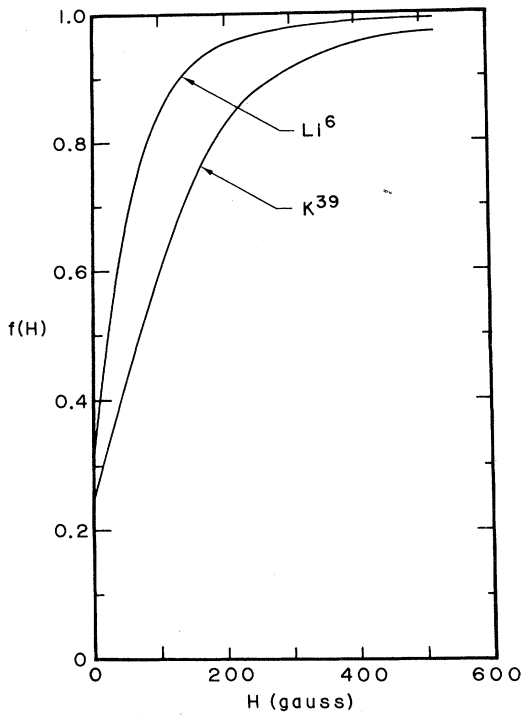

FIG. 2. The parameter $f(H)$ which describes the electronic polarization of high-field state-selected alkali atoms as function of the field H in the ionization region.

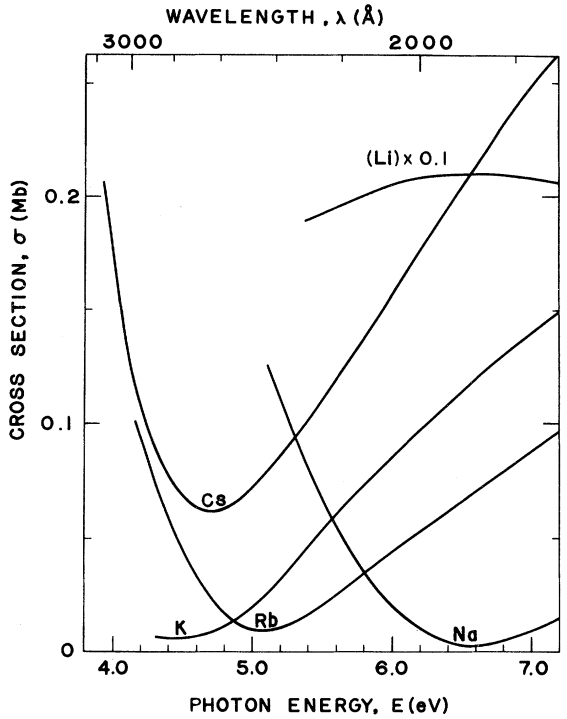

FIG. 3. Photoionization cross sections of alkali atoms. Best experimental values as given by Marr and Creek, Ref. 30. The cross-section minimum for K is closer to zero than shown in this figure, according to data of Hudson and Carter, Ref. 31.

indicate the approximate field strength required for obtaining $f(H) \gtrsim 0.9$.

C. Photoionization

We consider the photoionization of an alkali atom neglecting the effects of nuclear spin and hyperfine structure. The photoionization process is predominantly an electric dipole transition from the $n_0{}^2S_{1/2}$ ground state to a continuum P state designated by ϵP, where ϵ is the energy of the emitted photoelectron. The quantum-mechanical formula for the cross section is given by[29]

$$\sigma(E) = KE(1/\omega_A)\, S(A, B)\,, \tag{2.12}$$

where K is a constant, $E = E_{\rm th} + \epsilon$ is the photon energy, $E_{\rm th}$ being the threshold energy, $\omega_A = 2$ is the statistical weight of the initial state A, and $S(A, B)$ is the line strength of the transition to the state B, given explicitly by

$$S(A, B) = \sum_A \sum_B |\langle \psi_B(\epsilon P)|\, \mathcal{P}\, |\psi_A(n_0 S)\rangle|^2\,. \tag{2.13}$$

Here $\mathcal{P}$ is the electric dipole moment operator and the summations are taken over all degenerate levels of both the initial and final states. The wave function of the initial discrete state is normalized to $\langle \Psi_A | \Psi_A \rangle = 1$, whereas the wave function of the final continuum state is normalized to

$$\langle \Psi_B(\epsilon' P)|\, \Psi_B(\epsilon P)\rangle = \delta(\epsilon - \epsilon')\,. \tag{2.14}$$

Then if the line strength $S(A, B)$ is expressed in atomic units and the photon energy E is expressed in rydbergs, the constant K in Eq. (2.12) becomes $K = \frac{4}{3}\pi^3 \alpha a_0^2 = 2.69 \times 10^{-18}$ cm^2, where α is the fine-structure constant and a_0 is the Bohr radius. The energy dependence of the photoionization cross section $\sigma(E)$ is due to the factor E and also, more importantly, to the energy dependence of $\psi_B(\epsilon P)$, which strongly affects the matrix element. Experimental data on $\sigma(E)$ of the alkali atoms[30,31] are given in Fig. 3. As has been shown recently, the theory of alkali photoionization must also take into account the spin-orbit perturbation of the continuum P states.[32,5-7] We define radial matrix elements for transitions to the $j' = \frac{3}{2}$ and $j' = \frac{1}{2}$ continuum P states[5] as

$$R_3 = \langle \psi_B(\epsilon P; j' = \tfrac{3}{2})\, |\, \mathcal{P}\, |\, \psi_A(n_0 S)\rangle$$

and (2.15)

$$R_1 = \langle \psi_B(\epsilon P; j' = \tfrac{1}{2})\, |\, \mathcal{P}\, |\, \psi_A(n_0 S)\rangle\,.$$

The effects of the spin-orbit perturbation is taken into account by assuming the $R_3 \neq R_1$, where R_3 and R_1 are real functions of the photon energy E. The cross section can be written as

$$\sigma(E) = KE\{4[R_3(E)]^2 + 2[R_1(E)]^2\}$$

$$= \tfrac{4}{3} KE[R_3(E) - R_1(E)]^2 \{1 + \tfrac{1}{2}[X(E)]^2\}\,, \tag{2.16}$$

where

$$X(E) = \frac{2R_3(E) + R_1(E)}{R_3(E) - R_1(E)}\,. \tag{2.17}$$

First-order perturbation theory indicates that $(R_3 - R_1)$ is a slowly varying function of the photon energy E, whereas the measured photoionization cross sections, shown in Fig. 3, indicate that $X(E)$ and therefore $(2R_3 + R_1)$ vary rapidly and pass through zero in the vicinity of the cross-section minimum exhibited by all alkali atoms that are

TABLE I. Properties of one-electron atoms related to their electronic polarization after high-field state separation.

Atom	Abundance (%)	I	$f(H)$ at $H=0$	$\Delta W/\mu_B$ (G)
H^1	100	$\frac{1}{2}$	0.50	1015
H^2	...	1	0.33	234
Li^6	7.4	1	0.33	163
Li^7	92.6	$\frac{3}{2}$	0.25	574
Na^{23}	100	$\frac{3}{2}$	0.25	1266
K^{39}	93.2	$\frac{3}{2}$	0.25	330
K^{41}	6.8	$\frac{3}{2}$	0.25	182
Rb^{85}	72.2	$\frac{5}{2}$	0.17	2169
Rb^{87}	27.8	$\frac{3}{2}$	0.25	4883
Cs^{133}	100	$\frac{7}{2}$	0.13	6568

heavier than lithium.

The spin-orbit perturbation affects not only the cross-section curve but also the polarization of the outgoing photoelectron. The final states in the $|\epsilon P; l', s', j', m_j'\rangle$ representation, for which the transition matrix elements R_3 and R_1 apply, can be transformed through Clebsch-Gordan coefficients into the $|\epsilon P; l', s', m_l', m_s'\rangle$ representation, from which the photoelectron polarization can be calculated.[5] For the photoionization of polarized alkali atoms with unpolarized photons, the polarization of the free photoelectron follows from[7]

$$P_{e,\text{free}} = P_{e,\text{atom}} R(E) , \tag{2.18}$$

where $P_{e,\text{atom}}$ is the electronic polarization of the atom and $R(E) = X^2/(X^2+2)$. Quantitative theoretical calculations for $X(E)$ are not yet available; however, experimental data on $X(E)$ for K, Rb, and Cs have recently been obtained.[7,33]

D. Electron Extraction

The photoelectrons are produced in the volume where the atomic beam and the photon beam overlap. The electrons are polarized in the z direction, parallel to the ionizer magnetic field H_0. Their initial energy E_0 depends on the photon energy spectrum, and their directional distribution is that of a P wave with respect to the z axis, the direction of the incident photon beam.

For measurement of the electron polarization and for use of the polarized electrons in other experiments, a suitable electron beam outside of the magnetic field H_0 of the ionizer is necessary. Finding the optimum field configuration for electron extraction and beam formation is a technical problem which is discussed in Sec. IIIC for the requirements of our experiment.

The essential electron-optical property of the extracted electron beam is its phase-space volume.[34] For an electron beam of energy E, which is rotationally symmetric with respect to the z axis, the relevant information about its phase-space volume is given by its emittance

$$\epsilon = \rho\,\alpha , \tag{2.19}$$

in which ρ is the radius of the electron beam at an image of the electron source (or at the source itself) and α is the aperture angle; that is, half the apex angle of the cone which includes all the electron trajectories from one image point (or source point). Nonrelativistically, the emittance is proportional to $E^{-1/2}$ (E is equal to the final beam energy). The quantity I/ϵ^2 (where I is the beam current) is often referred to as "brightness" or *Richtstrahlwert*.[35] The importance of the emittance lies in the fact that for a given beam energy and current it is a constant beam parameter which cannot be reduced by electron-optical means.

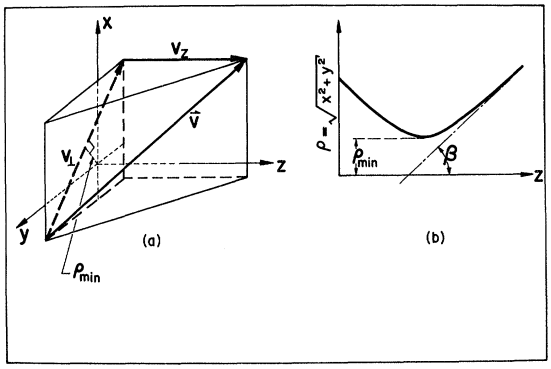

FIG. 4. Illustration of the skewing effect. An electron, produced at an off-axis point in the ionizer and extracted from the magnetic field will have a straight but skewed trajectory as shown in (a). The relevant parameters are ρ_{min} and the asymptotic angle β introduced in (b).

One of the possible field configurations for electron extraction is a homogeneous electric field in the z direction which accelerates the electrons in z direction without affecting the velocity components in x and y direction. After acceleration, the beam radius r is approximately given by ρ_0, the radius of the effective ionizer volume, and α is given by the ratio of radial and axial velocity component. Thus $\alpha \simeq (E_0/E)^{1/2}$, where E_0 is the average initial photoelectron energy. These estimates for ρ and α apply only to extraction in a homogeneous electric field. However, the emittance estimate given by the product of both,

$$\epsilon \simeq \rho_0 (E_0/E)^{1/2} , \tag{2.20}$$

is valid for all possible field configurations.

In the presence of the magnetic field H_0 at the source, the emittance given above is no longer an adequate description of the electron beam. The extraction from the ionizer magnetic field leads to a skewing of all off-axis trajectories which puts limitations on the beam characteristics similar to those imposed by the emittance.[28]

Assume that the electric and magnetic fields are axially symmetric and that the photoelectrons are produced with negligible initial velocities in the field H_0 at a maximum distance ρ_0 from the axis. After acceleration to the velocity v, the electrons are extracted from the magnetic field. Outside the magnetic field, all electrons produced off axis will have skewed trajectories. In field-free regions these trajectories will be straight lines having a minimum axial distance ρ_{min} and an asymptotic angle with respect to the axis β as shown in Fig. 4. Quantitatively this skewing effect can be treated by utilizing the fact that the axial component (L_z) of the canonical angular momentum of the electrons,

$$\vec{L} = \vec{r} \times (m\vec{v} - e\vec{A}) \tag{2.21}$$

(in which $\vec{r}$ is the radius vector, m is the mass, $\vec{v}$ is the velocity, e is the elementary charge, and $\vec{A}$ is the magnetic vector potential), is a constant of motion.[36] For electrons in axially symmetric fields this can be written as

$$L_z(z,\rho) = m\rho^2\frac{d\phi}{dt} - \rho e\left(\tfrac{1}{2}\rho H(z,0) - \tfrac{1}{16}\rho^3\frac{d^2H(z,0)}{dz^2} + \cdots\right) = \text{const}, \quad (2.22)$$

where ϕ is the azimuthal angle, t is the time, and H is the magnetic field. In the ionizer the electron velocity is assumed to be zero initially and, therefore,

$$L_z(\rho_0, H_0, v_0 = 0) = -\tfrac{1}{2}e\rho_0^2 H_0, \quad (2.23)$$

where the higher-order terms in Eq. (2.22) have been neglected. After extraction from the field, L_z is given by

$$L_z(\rho, H = 0, v \neq 0) = m\rho_{\min}\left[\rho^2\left(\frac{d\phi}{dt}\right)^2 + \left(\frac{d\rho}{dt}\right)^2\right]^{1/2} = m\rho_{\min}v_\perp, \quad (2.24)$$

in which $v_\perp$ is the velocity component orthogonal to the z axis. For $\rho \gg \rho_{\min}$, v approaches $v_z\tan\beta$. Usually, the asymptotic angle β is small with a consequence that $\tan\beta \sim \beta$ and $v_z \sim v$. Hence from the invariance of L_z it follows that

$$\rho_{\min}\beta = \tfrac{1}{2}(e/m)\rho_0^2 H_0/v, \quad (2.25)$$

where the product $\rho_{\min}\beta$ is the so-called skew parameter and is proportional to $E^{-1/2}$ as is the emittance which was discussed above.

For our electron source, where the electrons originate in the magnetic field H_0, but the electron beam is used outside the field H_0, it is necessary to introduce the concept of a generalized emittance ϵ which includes the skewing effect. For the purpose of an estimate it is sufficient simply to add $\rho_{\min}\beta$ to the emittance $\rho\alpha$, and thus obtain

$$\begin{aligned}\epsilon^* &\simeq \rho_0(E_0/E)^{1/2} + \tfrac{1}{2}(e/m)\rho_0^2 H_0/v \\ &= \rho_0(v_0/v)\left[1 + \tfrac{1}{2}(e/m)\rho_0 H_0/v\right] \\ &= \rho_0(v_0/v)\left[1 + \tfrac{1}{2}\rho_0/\rho_0^*\right], \end{aligned} \quad (2.26)$$

where $\rho_0^* = mv_0/eH_0$ is the radius of curvature of electrons with velocity v_0 in the field H_0, if $\vec{v}$ is orthogonal to $\vec{H}_0$. In our experiment the skewing effect contributes the major portion of ϵ^*.

E. Electron Polarization Analysis

For our experiment the most suitable method of measuring the electron polarization is Mott scattering.[37] This scattering exhibits a large electron-spin dependence for wide-angle scattering from heavy nuclei at electron energies on the order of 100 keV. Since the spin dependence arises from spin-orbit interaction, the electron beam to be analyzed must have a transverse polarization, orthogonal to the plane of scattering.

In the literature on polarization analysis by Mott scattering, the magnitude of the analyzing power is given by a function $S(\theta, E, Z)$ which depends on the polar scattering angle θ, electron energy E, and atomic number Z of the target material. The sign of the function S is the same as that of $(\vec{p}_1\times\vec{p}_2)\cdot\vec{A}$, where $\vec{p}_1$ and $\vec{p}_2$ are the electron momenta before and after the scattering, respectively. Figure 5 shows $S(\theta)$ for $Z = 79$ and $E = 100$ keV. Both theoretical curves result from essentially the same kind of Hartree potential calculation.[38,39] Note that radiative corrections are negligible at 100 keV.[40] The two experimental data points[41,42] in Fig. 5 indicate that theory and experiment agree reasonably well.

III. APPARATUS AND EXPERIMENTAL PROCEDURE

A schematic diagram of the experimental arrangement is given in Fig. 6. A beam of polarized alkali atoms was ionized by unpolarized uv light. The electrons were extracted from the ionizer while the positive ions drifted to a negative electrode. The electron intensity and polarization were then measured. In the following sections, the details of the experimental apparatus and procedure are discussed.

A. Atomic Beam System

1. *Experimental Arrangement*

Our work was done with both potassium and lithium atoms. Initially potassium was used because a potassium beam is easily produced and detected and because potassium has a low ionization potential and a low hfs splitting (Table I). Later Li^6 was used, principally because it has a high photoionization cross section and a very low hfs splitting.

The layout of the atomic beam system used for the lithium work is shown schematically in Fig. 7. (Also see Fig. 18 for a more detailed drawing.) The atomic beam was produced by vaporization of the alkali metal in an oven machined out of Armco iron which is the most resistive material for use with lithium metal.[43–45] Thermal radiation losses necessitated the use of a material with a low emissivity. Therefore, the oven was covered with molybdenum sheet metal. As a further protection against radiation loss, the oven was surrounded by a thermally insulated molybdenum shield. The heating elements for the oven consisted of tungsten spirals inside alumina tubes. A power input of 250 W was required for operation at a temperature of about 1000 °K. The oven had an orifice of 1.6-mm diameter, and the operating vapor pressure in the oven was approximately 0.4 Torr. With 2 g of lithium metal, the oven could be run for about 10 h.

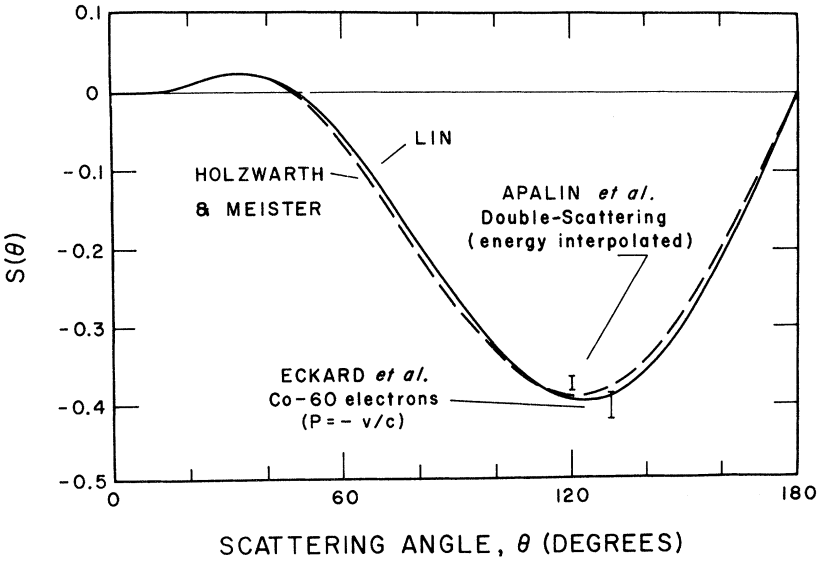

FIG. 5. Polarization sensitivity S versus scattering angle θ for scattering of 100-keV electrons from screened gold nuclei, calculated by Lin (Ref. 38) and Holzwarth and Meister (Ref. 39) and compared with data of Apalin *et al.* (Ref. 41) and Eckardt *et al.* (Ref. 42).

The oven was mounted such that alignment in the plane transverse to the atomic beam was possible during operation. Excessive condensation of lithium on the walls of the vacuum chamber was prevented by a demountable water-cooled housing which was placed around the entire oven assembly.

Lithium atoms energing from the oven passed through a 1.6-mm-diameter collimator. The collimator, as well as the housing of the electromagnetically activated beam flag, was maintained at a temperature of approximately 700 °K, to prevent condensation of lithium. The atomic beam intensity was monitored by a hot-wire detector located about 80 cm from the oven, downstream from the six-pole magnet and ionizer. The detector could be moved out of the beam line. The atomic-beam profile and flux measurements, described below, were performed with another hot-wire detector which was inserted at the location of the ionizer.

A permanent six-pole magnet shown in Fig. 8 was used for the state selection of the atomic beam.[46,20] The field in the magnet gap was not measured in detail throughout the gap. However, a measurement between adjacent pole tips yielded a field-strength value of 8500 G.

2. *Calculation of Magnet Properties*

The focusing and state-selection properties of the six-pole magnet can be calculated (see Appendix A) from the trajectory equation with the following two simplifying assumptions: (1) The inhomogeneous magnetic field in the magnet gap is an ideal six-pole field. (2) The magnetic moment of the atoms is $\mu \simeq \pm \mu_B$, which is a good approximation in strong magnetic fields (cf. Fig. 1) where the magnetic force on the atoms is significant.

The focusing and state-selecting properties of the magnet depend on the atom velocity v. For calculation of the beam intensity transmitted by the magnet, the appropriate velocity-distribution func-

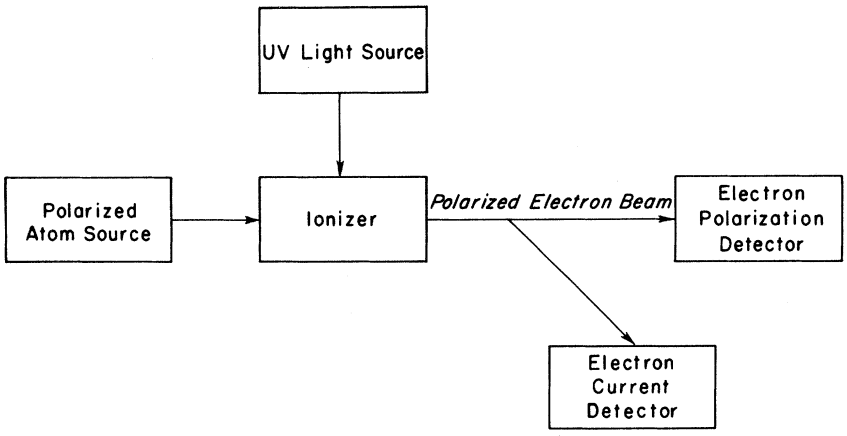

FIG. 6. Block diagram of the experimental arrangement.

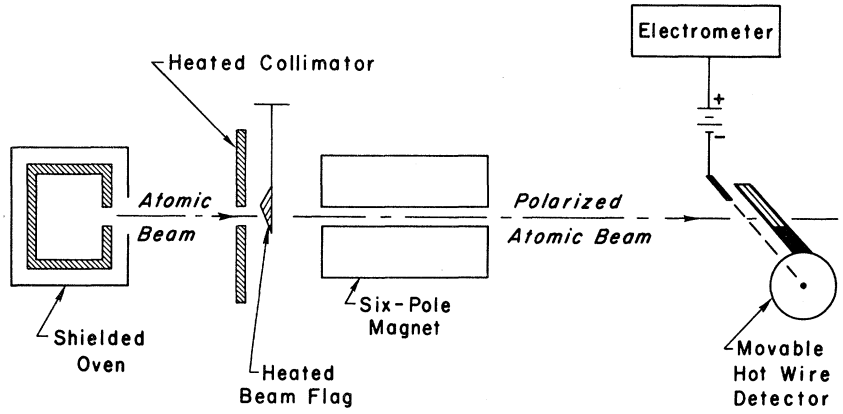

FIG. 7. Schematic diagram of the atomic beam arrangement (not to scale).

tion F_{BEAM} is the Maxwellian containing the factor v^3. On the other hand, $F_{\mathrm{GAS}} \propto (1/v) F_{\mathrm{BEAM}}$ is the relevant distribution function for calculation of the photoelectron current which depends on the atom *density* in the ionization region. Both distribution functions, expressed in terms of the inverse-velocity parameter $\eta = (4kT/m)^{1/2}/v$, where k is Boltzmann's constant, T is the temperature, m is the atomic mass, are plotted in Fig. 9.

The transmission characteristics of the magnet can be expressed in terms of two transmittance solid angles Ω^+ and Ω^-, corresponding, respectively, to the two electronic spin states $m_J = +\frac{1}{2}$ and $-\frac{1}{2}$. These solid angles, both of which are functions of η, were calculated for our experimental conditions and are plotted in Fig. 10. They refer to a point source on axis; the off-axis corrections necessary for a finite source as used in our experiment are negligible (see Appendix B).

The state-selection parameter s was defined in Eq. (2.8) in terms of N^+ and N^-, the number of atoms present in the ionizer in the electronic state $m_J = +\frac{1}{2}$ and $-\frac{1}{2}$, respectively. These numbers which are proportional to the corresponding transmittance solid angles averaged over the distribution function F_{GAS} are given by

$$N^{\pm} = (\mathrm{const}) \int_0^{\infty} F_{\mathrm{GAS}}(\eta)\, \Omega^{\pm}(\eta)\, d\eta \ . \qquad (3.1)$$

The state-selection parameter is plotted in Fig. 11 as function of the magnet length for two different oven temperatures.

Six-pole magnets can yield perfect state selection if a central beam stop is inserted at the magnet entrance such that the magnet exit lies in the shadow of the stop. This technique has been used in experiments on atomic spectroscopy.[47,48] The atomic beam flux, however, is severely reduced by a central beam stop because the stop reduces Ω^+ and the shadow condition restricts the source radius to a very small value. Hence a beam stop

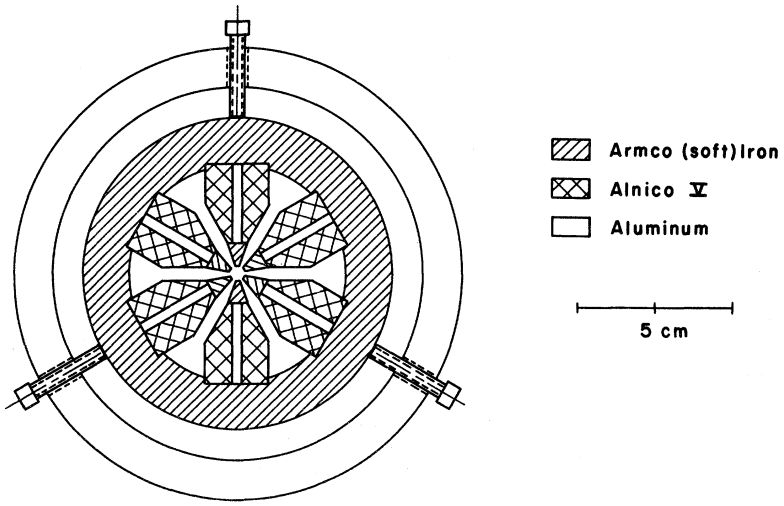

FIG. 8. Cross section of the permanent six-pole magnet.

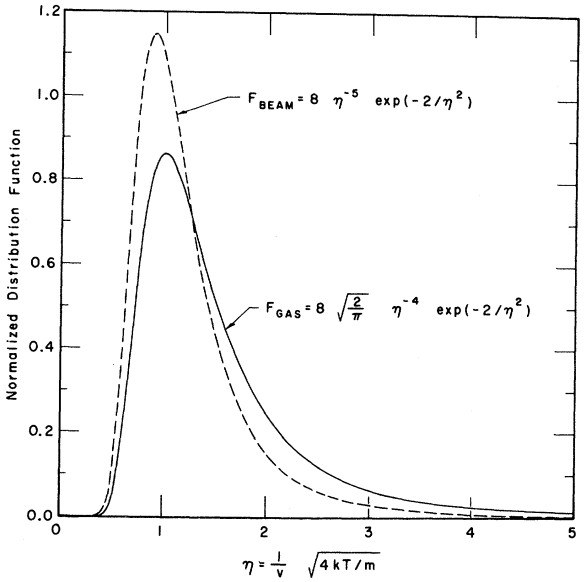

FIG. 9. Thermal equilibrium distribution of atoms in a gas and in a beam, plotted as a function of the inverse-velocity parameter η.

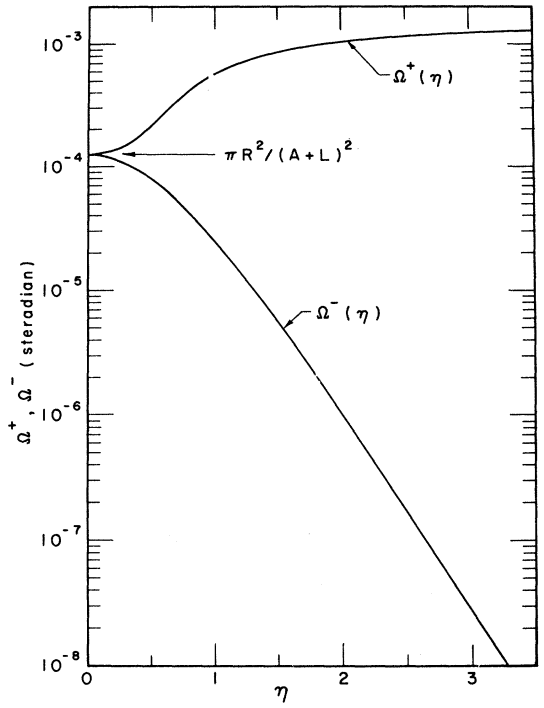

FIG. 10. Transmittance solid angles of the six-pole magnet calculated for the conditions of our experiment. The relevant parameters are the following: distance, oven to magnet entrance, $A = 7.3$ cm; length of magnet, $L = 17.5$ cm; magnet gap radius, $R = 0$, 16 cm; magnetic field at radius R, $H_R = 8500$ G.

was not used in our experiment.

The number of atoms per second ϕ which leave a source of pressure p and orifice radius R_s within the solid angle Ω_ϕ is given by[49]

$$\phi = c\,\Omega_\phi\, p\,\pi R_s^2/(TM)^{1/2}\,, \qquad (3.2)$$

where T is the source temperature, M is the molecular weight, and $c = 1.115\times10^{22}$ (°K amu)$^{1/2}$/(Torr cm^2 sr sec). The atom flux transmitted by the six-pole magnet follows from Eq. (3.2) with

$$\Omega_\phi = \int_0^\infty F_{BEAM}(\eta)\,\tfrac{1}{2}\,[\Omega^+(\eta)+\Omega^-(\eta)]\,d\eta\,. \qquad (3.3)$$

For the conditions of the lithium experiment (where $p = 0.4$ Torr) we calculated $\phi = 3.7\times10^{14}$ atoms/sec and $\Omega_\phi = 3.2\times10^{-4}$ sr. Note that as a result of the focusing action of the magnet, Ω_ϕ is 2.5 times greater than the solid angle subtended by the magnet exit at the source.

3. *Majorana Transitions*

In a six-pole magnet the atomic states adiabatically follow the magnetic field seen by the atom, provided the field is not close to zero where nonadiabatic (Majorana) transitions can occur.[50,27] We estimate that the nonadiabatic transitions are negligible in our experiment for the following reasons: (1) The critical region close to the axis, where nonadiabatic transitions may occur, has a radius of $r_{crit} \lesssim 10^{-2}R$. (2) Because of the finite source size, very few atoms traverse this critical region. (3) The ionizer magnetic field penetrates into the six-pole magnet gap, so that the field on the axis is not zero. This field penetration also facilitates the adiabatic transfer into the ionizer field without the need for further precautions such as a specially shaped transition field.

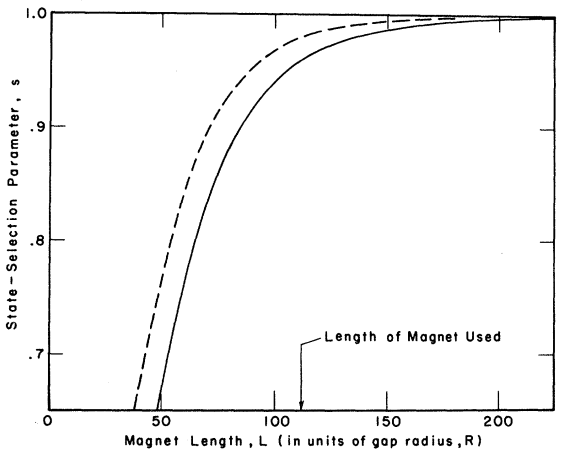

FIG. 11. State-selection parameter as function of magnet length, calculated for the design parameters used in this experiment. The solid curve refers to a source temperature of 970 °K (as in the lithium experiment); the dashed curve, to 650 °K (as in the potassium experiment).

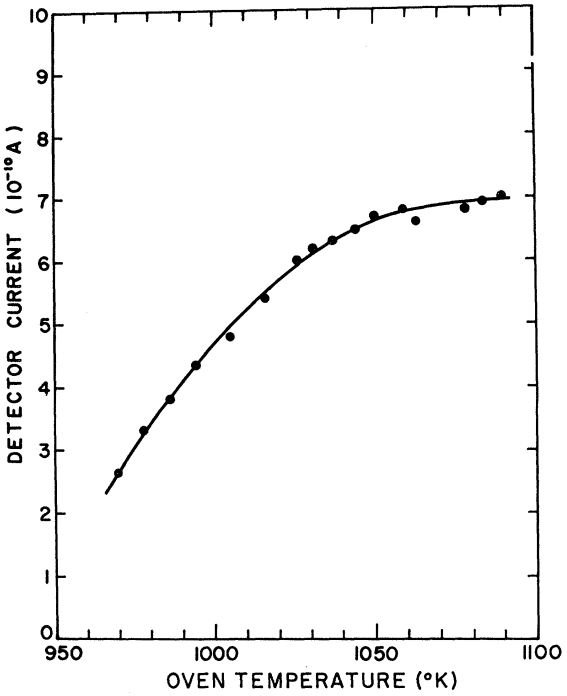

FIG. 12. Intensity of the lithium atomic beam as function of the oven temperature, measured at the ionizer.

4. *Atomic Beam Measurements*

The efficiency of a surface-ionization detector for converting the alkali atoms incident on the hot wire into ions to be collected by a negatively biased electrode is given by[51,52]

$$\zeta = n_+/n_0 = 1/(1+2e^{-e(I-\varphi)/kT}) , \qquad (3.4)$$

where n_+ is the number of ions, n_0 the number of incident alkali atoms, e the elementary charge, I the ionization potential of the atoms, φ the work function of the wire material, k Boltzmann's constant, and T is the temperature of the wire which has to be sufficiently high to avoid condensation of alkali atoms.

With a hot-wire detector mounted at the position of the ionizer and with the six-pole magnet in place, the detector signal was measured as function of the oven temperature. The data for lithium are shown in Fig. 12. As expected for an effusion beam, the intensity increases with oven temperature but then starts to level off because of increasing atom-atom scattering in the dense beam in front of the oven orifice. The oven operating temperature for lithium was 970 °K, corresponding to the lowest point in Fig. 12. The higher intensity at higher temperature could not be utilized in our investigations because excessive lithium condensation produced instabilities in the beam and caused the beam flag to stick frequently. A curve similar in shape to that of Fig. 12 was obtained for the potassium beam intensity versus oven temperature. The operating oven temperature for potassium was 620 °K and was also well below the levelling-off region.

For measurement of the atomic beam profile, a vertical hot-wire detector was moved transverse to the atomic beam by means of a micrometer drive coupled to a rotary vacuum feed through. The exposed length of the wire was 1.1 cm, well in excess of the vertical extension of the atomic beam. The 0.01-cm wire diameter was small compared to the beam width. A typical beam profile for the lithium beam, taken with an oven temperature of 970 °K is shown in Fig. 13. The full width at half-maximum (FWHM) is 0.165 cm, which is only about one-half of the magnet gap diameter. For the potassium beam, we measured a profile with FWHM of 0.26 cm. The focusing action of the six-pole magnet, which depends on the atom velocities and thus on the oven temperature, was different for lithium and potassium. Therefore the profile widths were different for lithium and potassium.

A measurement of the absolute beam flux requires knowledge of the hot-wire detection efficiency ζ. For the measurements on potassium we used a platinum wire. In that case the work function is larger than the ionization potential and ζ is close to unity[52] at typical wire operating temperatures of about 1200 °K. Integration over the potassium beam profile obtained with an oven temperature of

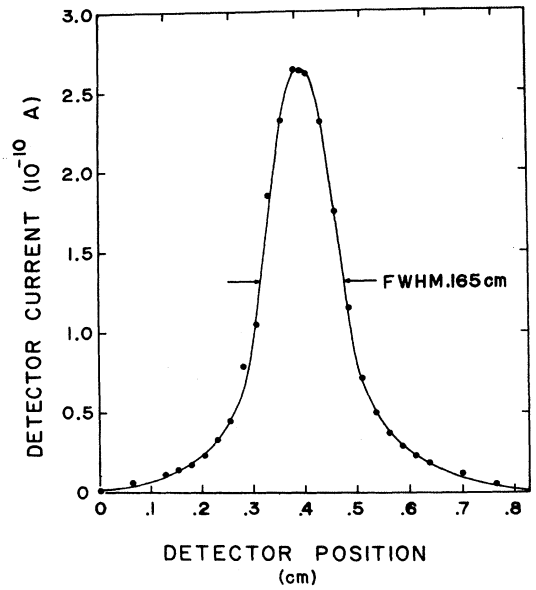

FIG. 13. Measurement of the lithium beam profile at the ionizer by means of a movable hot-wire detector with a 0.1-mm-diam iridium wire. The wire temperature was 1645 °K, for which the detection efficiency was determined as $\zeta = 1\times10^{-4}$ (±50%).

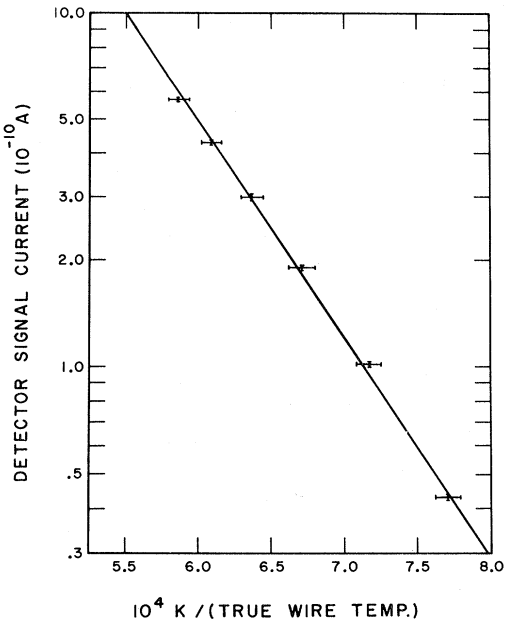

FIG. 14. Dependence of detector signal on hot-wire temperature, for a constant incident lithium beam. From the slope of the solid line the work function of the iridium wire was determined and hence the detection efficiency as a function of temperature.

620 °K yielded a beam flux of 7×10^{13} atoms/sec.

Lithium has an ionization potential[53] of 5.39 V, which is significantly higher than the 4.34-V ionization potential of potassium. For $\varphi \lesssim I$ the detection efficiency depends strongly on the work function φ. We therefore used iridium as the material for the hot wire since its listed work function[54] of 5.3 V is very high. Because the work function depends on the crystal structure of the wire material, we did not rely on the literature value for φ but instead calibrated the hot-wire detector from measurements of the detector signal as functions of the wire temperature, measured pyrometrically, while the oven temperature was held constant. These calibration measurements are plotted in Fig. 14. The straight line represents the best fit to the data and corresponds to an iridium work function of 4.15 eV (±10%) which is much lower than the literature value. The efficiency ζ varied from 9×10^{-6} (±50%) at a wire temperature of 1250 °K to 1.2×10^{-4} (±50%) at 1700 °K. With ζ thus determined, integration over the lithium beam profile of Fig. 13 yielded a beam flux of $\phi = 3.2\times10^{14}$ atoms/sec (±50%) in good agreement with the calculated value of $\phi = 3.7\times10^{14}$ atoms/sec.

B. Optical System

The light source used in the work with potassium was a mercury high-pressure dc arc (Osram HBO 200 W/2). For the continuous photoionization of lithium, the light source was a xenon-mercury high-pressure arc lamp with Suprasil envelope (Hanovia 910B-1, special order). Since the lamp was mounted inside the optics chamber (cf. Fig. 16) where cooling by free convection was not sufficient, variable forced-air cooling was employed while the temperature of the upper lamp socket was monitored by means of a thermocouple. For the pulsed photoionization of lithium, the light source was a condensed high-voltage spark discharge between tungsten electrodes placed about 1 mm apart in 7 atm of argon or xenon. The pulsing circuit operated at repetition rates up to 10 sec^{-1} and dissipated about 5 J per flash. A cross section of the spark light source is shown in Fig. 15.

The optical arrangement is shown in Fig. 16. The light from the lamp was focused by a 23×23 cm spherical, aluminized front-surface mirror with an MgF_2 protective coating. A 7.6-cm-diam Suprasil quartz window, 0.6 cm thick, separated the optics chamber from the vacuum system. Inside the vacuum system, the converging light was reflected through 90° by a plane, aluminized, front-surface mirror with an MgF_2 coating. In the center of the mirror, a 0.47-cm-diam hole was cut to allow the atomic beam to pass through and reach the ionizer. Inside the ionization region where light and atomic beam overlap, an image of the light source magnified about four times was produced.

The mirror for the 90° reflection of the light beam was heated to about 700 °K by a Nichrome heater incorporated into the mirror mount, in order to prevent condensation of diffusion pump oil and alkali vapor on the front surface of the mirror. It was observed in the earlier potassium experiment that film formation on an unheated mirror seriously reduced the uv reflectivity. Also, in the earlier work we observed deterioration of the plane mirror and the window which resulted from their exposure to electrical discharges occurring during conditioning of the high-voltage system. In the lithium experiment both the plane mirror and the window were well hidden inside metal enclosures, thus preventing exposure to discharges. As a consequence, no deterioration was observed.

At the beginning of our work, we attempted to utilize multiple light reflection in an ionizer configuration similar to that used by Friedmann.[2] Disappointing results led us to abandon this approach[55] in favor of the simpler configuration shown in Fig. 16.

The light intensity was monitored as a check on the stability and long-time performance of the light source. Optimization of the optical arrangement was achieved by measurement of the photoelectron current obtained. No absolute light intensity measurements were attempted.

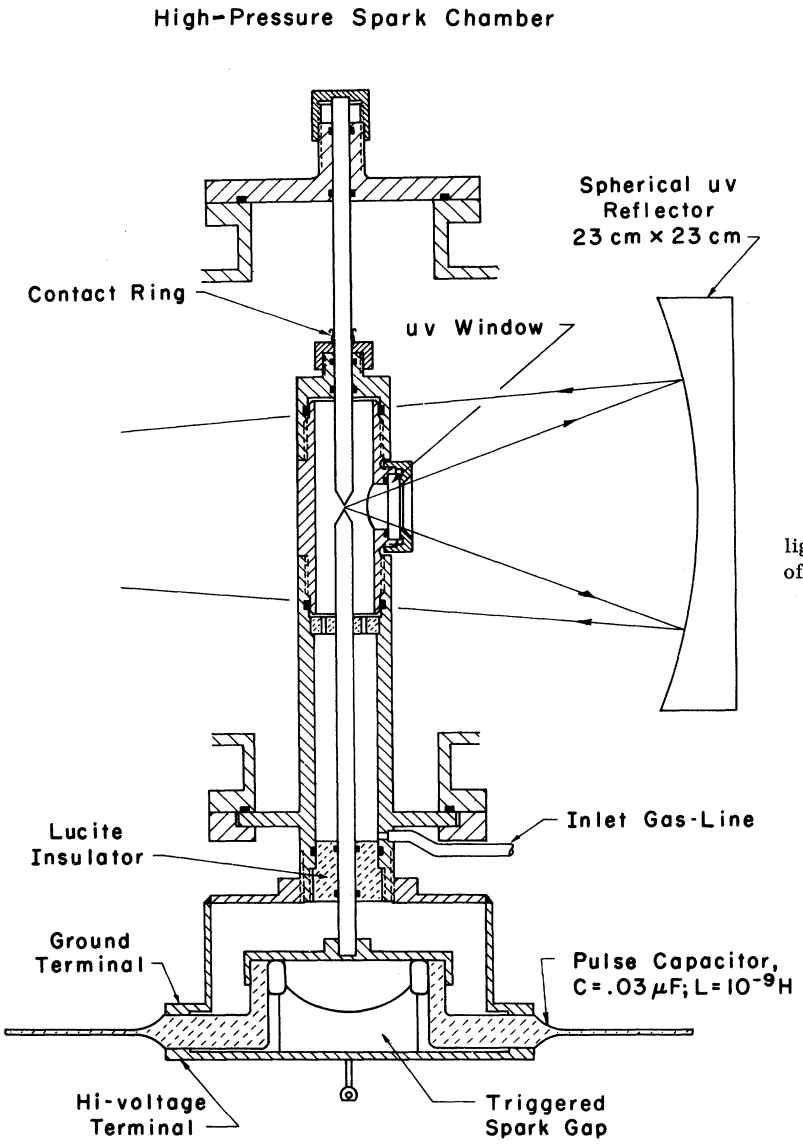

FIG. 15. Cross section of the spark light source used for pulsed photoionization of lithium.

C. Electron-Optical System

1. *Arrangement*

The major electron-optical components are shown schematically in Fig. 17 and also in the scale drawing of the assembly given in Fig. 18. Both the atomic beam and the light beam go axially from left to right. Most of the photoelectrons are created where the small light source is imaged onto the atomic beam.

For measurement of electron polarization we required a beam energy of about 100 keV. In our experiment, the Mott scattering polarization detector was at ground potential and the ionizer, at −100 kV. Substantial developmental work was done to solve all the high-voltage insulation problems in order to obtain a compact and convenient source of polarized electrons.

High-voltage discharges were prevented through the use of highly polished metal parts in the ionizer whose edges were beveled with a minimum radius of curvature of 5 mm. The high-voltage region was supported by three Supramica (Mycalex Corporation) insulating rods (see Fig. 18) into which ridges had been machined to reduce the possibility of gliding discharges. After machining, the insulators were polished under water. The high-voltage contact to the ionizer was made through an oil-filled ceramic feed through. The high voltage was measured with the aid of a calibrated resistor with corona and leakage protection, connected to a microammeter at ground potential. An axial magnetic field in the ionizer is needed to decouple the electronic and nuclear spins of the alkali atoms.

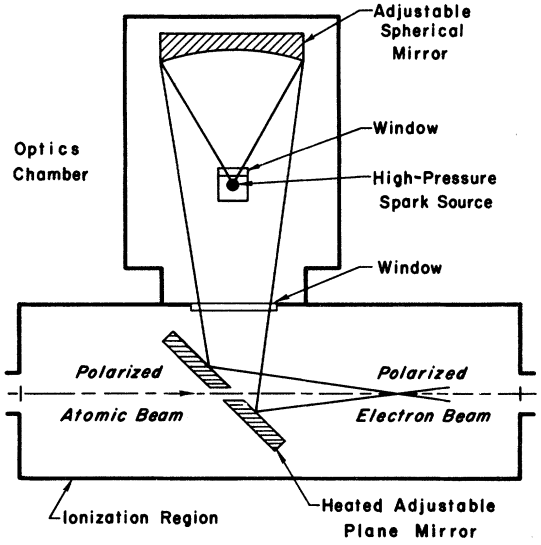

FIG. 16. Schematic diagram of optical arrangement (not to scale).

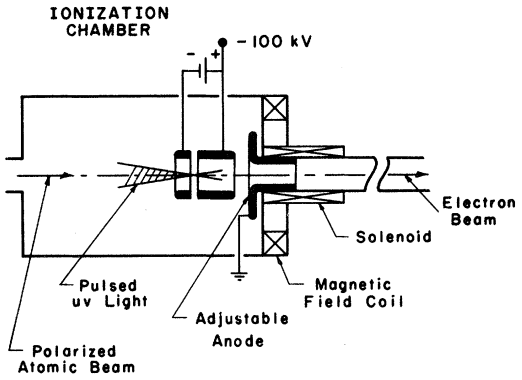

FIG. 17. Schematic diagram of electron-optical arrangement (not to scale).

The direction of the field determined the direction of polarization of the photoelectrons. For space considerations rather than electron-optical reasons, the big magnetic field coil was installed at an axial position 18 cm downstream of the ionizer. The photoelectrons were accelerated between the ionizer and the grounded anode (see Fig. 17). A repeller electrode at - 500 V with respect to the ionizer prevented the electrons from leaving the ionizer at the other end.

2. *Tests*

A copper mesh mounted on a bow which could be

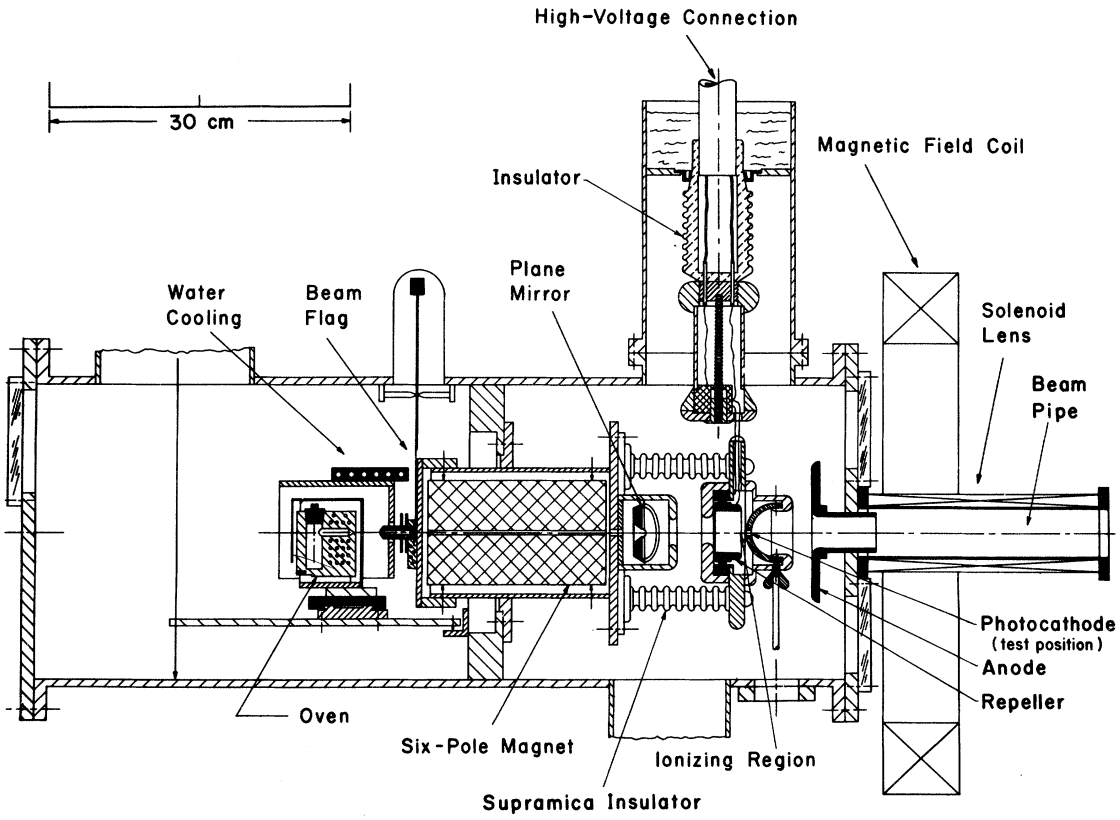

FIG. 18. Scale drawing of the polarized electron source assembly.

pivoted into the center of the ionizer served as photocathode for tests and adjustments of the electron-optical system. For the initial studies of the electron optics, a thermionic electron source, consisting of a heated tungsten helix, was mounted in the center of the ionizer and the trace of the electron beam was observed on a luminescent screen mounted at the end of the beam pipe. We found that suitable beam formation was achieved with 100 kV between ionizer and anode and with the coil producing a magnetic field of 200 G in the center of the coil and about 100 G in the ionizer. We later introduced a solenoid to obtain suitable beam transport with reduced magnetic field in the ionizer in order to measure the electron polarization as a function of the ionizer magnetic field.

3. *Trajectory Calculation*

As a supplement to the experimental studies of the electron beam optics. we calculated electron trajectories for a field configuration similar to that of our experiment. We used a step by step integration of the nonrelativistic force equations for charged particles in axially symmetric electric and magnetic fields.[36] We made the calculations in second-order approximation, which is the next order beyond the paraxial approximation, and we did not restrict the calculations to meridional trajectories. The radial coordinate ρ, which is independent of azimuthal angle, was plotted on a Calcomp plotter as function of the axial coordinate z. The center of the ionizer is $z = 0$. Some results of the trajectory computations are shown in Fig. 19.

The electric potential distribution along the axis $V(z)$ and the magnetic field on the axis $H(z)$, which are plotted in Fig. 19(a), define the model on which our calculations were based. The electric potential function is an approximation[56] for two cylinders at potentials 0 and ΔV, respectively, with the following dimensions: cylinder radii, 1.9 cm; gap between the cylinders, 2.1 cm; center of the gap at $z = 5.7$ cm. The magnetic field function is that of a loop at $z = 18$ cm with a loop radius of 22 cm.

The trajectories of Fig. 19(b) all start at $z_0 = 0$ and $\rho_0 = 0.25$ cm and with zero initial energy $E_0 = 0$. They correspond to magnetic fields which vary from $H_{max} = 0$ to $H_{max} = 250$ G in steps of 50 G. The potential function is that of Fig. 19(a) with $\Delta V = 100$ kV for all trajectories. The trajectory for $H_{max} = 200$ G, with a minimum of ρ at $z \approx 43$ cm, comes very close to the electron-optical requirements for our experiment. For the trajectories of Fig. 19(c) and 19(d), $H_{max} = 200$ G was held constant while other parameters were varied. The trajectories of Fig. 19(c) differ in the initial axial coordinate z_0. The range from $z_0 = -2$ cm to $+2$ cm corresponds approximately to the overlap of atomic beam and light beam in our experiment. The plot of Fig. 19(c) shows that the form of the trajectories is not very sensitive to variations in z_0. The last plot, Fig. 19(d), shows trajectories which start at $z_0 = 0$, $\rho_0 = 0.25$ cm with an initial energy $E_0 = 2$ eV, which is about the maximum energy of the photoelectrons, produced in our experiment. Six different directions for the initial velocity were selected. The sixth trajectory, which starts backward in axial direction, stops inside the ionizer because the limit for calculation steps set in the program had been reached. The other five trajectories show that suitable beam formation, with a minimum of ρ near $z \approx 43$ cm, can be achieved even if the electrons have initial energy of 2 eV and different initial velocity directions.

The results of the trajectory computations for the field-model resembling our experimental arrangement are in good agreement with our experimental observations.

D. Current Measurements

After leaving the ionization region, the electron beam entered a pipe, approximately 1 m long, which led to the polarization measuring apparatus (cf. Sec. III E). The beam pipe consisted of several components, each having an inside diameter of about 5 cm. One portion of the pipe, between the ionization chamber and the electrostatic deflector, contained the movable hot-wire detector used for monitoring the atomic beam intensity. Downstream from the hot-wire detector was a section which housed a Faraday cage for electron current measurements. Measurement of the electron current is nontrivial since not only electrons but also alkali atoms and uv photons are incident on the cage. In addition, the cage is located in the magnetic field of the big coil. To keep secondary electrons in the cage, a negatively biased electrode was inserted at the entrance and was shielded from uv light by a grounded disk. A door at the rear of the cage could be opened to allow the beam to enter the polarization analyzer.

E. Electron-Polarization Measurements

1. *Polarization Conversion*

An electrostatic deflector was employed to convert the longitudinal polarization of the electron beam into the transverse polarization required for polarization analysis. The deflecting plates of the polarization converter were 5-cm-high concentric aluminum cylinders of mean radius 25 cm, separated by a distance of 0.82 cm and having an arc length of 112°. For 100-keV electrons, the beam leaving the converter has a nearly perfect transverse polarization.

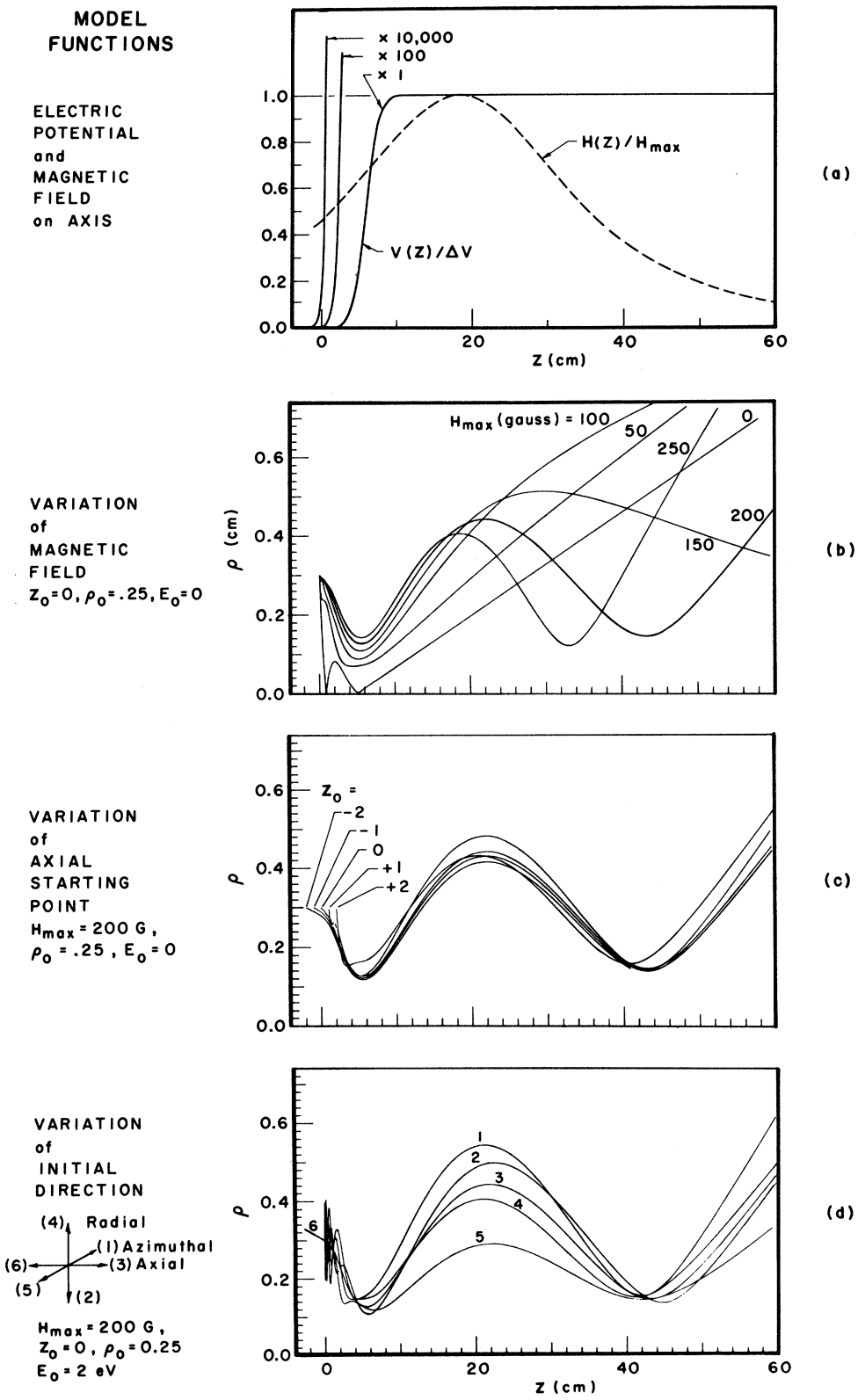

FIG. 19. Results of trajectory calculations for a polarized electron source model. Plot (a) gives the axial distributions of electric potential and magnetic field which describe the model. Plots (b)–(d) show trajectories computed for various conditions as indicated on the left-hand side. Note that the scales for z and ρ are different.

2. *Mott Scattering Technique*

A scattering chamber for scattering through an angle of $\theta = 118°$ was used. Early measurements with scintillator-photomultiplier detectors showed that improved energy resolution was necessary for efficient discrimination against electrons scattered from the walls. As a result, silicon surface-barrier junction detectors were employed. They were mounted 180° apart in azimuthal angle in a rotable housing whose axis of rotation coincided with the direction of the incident electron beam. The output pulses from the detectors were amplified and shaped with charge-sensitive preamplifiers and low-noise amplifiers. The signals were then routed to alternative halves of a 400-channel pulse-height analyzer. The pulse-height spectrum was read out onto paper tape, converted to punched cards, and processed on a computer.

A collimator with a 0.64-cm-diam hole, located in front of the scattering foil, ensured that electrons hit only the foil and not the foil holder. Other collimators within the scattering chamber reduced the likelihood that electrons scattered by the walls could reach the detectors. In addition, the collimators and walls were coated with graphite to increase the probability of energy loss in wall collisions.

Along the 2-m path from the ionizer to the polarization measuring apparatus, magnetic steering fields were used to maximize electron transmission and to control the angle of incidence of the beam on the scattering foil. A second Faraday cage, located beyond the scattering foil, monitored the electron beam at the polarization measuring apparatus. The electron current measured in this cage was typically 25% of that measured in the first Faraday cage. With the deflector voltage held constant, the electron current in the second cage was a sharply peaked function of the main accelerating voltage. The peak occurred at 100 kV and had a FWHM of 2 kV, as compared to 3 kV calculated for the transmission of the electrostatic deflector which served as a polarization converter. Thus the electrostatic deflector did not seriously restrict the beam transmission.

The scattering foils with a diameter of 1.9 cm, were mounted on a wheel that could be rotated under vacuum to place any one of four foils in position. The foils used were the following: aluminum with a thickness of approximately 1 mg/cm^2; gold of different thicknesses up to 105 μg/cm^2, evaporated onto Formvar backings; and a bare Formvar foil with a thickness of approximately 20 μg/cm^2.

Low molecular weight Formvar[57] was dissolved in ethylene dichloride at a concentration of 8 g/liter. A clean microscope slide was dipped into the Formvar solution and withdrawn quickly and smoothly after several seconds. The end of the dripping slide was blotted on absorbent paper in order to remove the excess solution and draw the film out evenly. After the slide had dried, the edge of a razor blade was used to cut out the area of the film to be used as the target backing. Next, the slide was breathed upon until it became fogged. Then it was immersed in a pan of water and the film was floated off. A mounting ring was finally inserted under the film and both ring and film were removed from the water. Then gold was evaporated in vacuum and deposited onto the Formvar foil. A piezoelectric deposit monitor[58] was used to measure the thickness of the gold layer.

3. *Method of Data Taking*

The Mott scattering plane in which the two electron detectors A and B lie is the vertical plane through the axis of the incident horizontal beam. The ratio of the counts registered in the two detection channels, C_A/C_B, is called R_0 if the detector A is in top position and R_π if the scattering chamber is rotated around the beam axis through 180° so that detector B is in top position. If δ' is the scattering asymmetry as yet uncorrected for any instrumental asymmetries, and if η_A and η_B are the detection efficiencies of the detectors A and B, then R_0 and R_π are given by

$$R_0 = (\eta_A/\eta_B)\,(1-\delta')/(1+\delta')\,,$$
$$R_\pi = (\eta_A/\eta_B)\,(1+\delta')/(1-\delta')\,, \tag{3.5}$$

and

$$(1-\delta')/(1+\delta') = (R_0/R_\pi)^{1/2}\,.$$

Rotation of the detector housing (including the scattering foil) can introduce another asymmetry if the axis of rotation is at an angle with respect to the incident electron beam. The rotational asymmetry ρ and the polarization asymmetry δ both enter into the observed asymmetry δ'. For measurements with a gold scattering foil these asymmetries are related according to

$$(1-\delta'_{\mathrm{Au}})/(1+\delta'_{\mathrm{Au}}) = [(1-\delta_{\mathrm{Au}})/(1+\delta_{\mathrm{Au}})] \times[(1-\rho_{\mathrm{Au}})/(1+\rho_{\mathrm{Au}})]\,, \tag{3.6}$$

or, to a good approximation for small asymmetries,

$$\delta'_{\mathrm{Au}} \simeq \delta_{\mathrm{Au}} + \rho_{\mathrm{Au}}\,. \tag{3.7}$$

For the elimination of the rotational symmetry, an aluminum scattering foil was used for which the function $S(\theta, E)$ is very close to zero. In this case the measured asymmetry δ'_{Al} is given by

$$\delta'_{\mathrm{Al}} = \rho_{\mathrm{Al}}\,. \tag{3.8}$$

The relationship between ρ_{Al} and ρ_{Au} was determined experimentally as

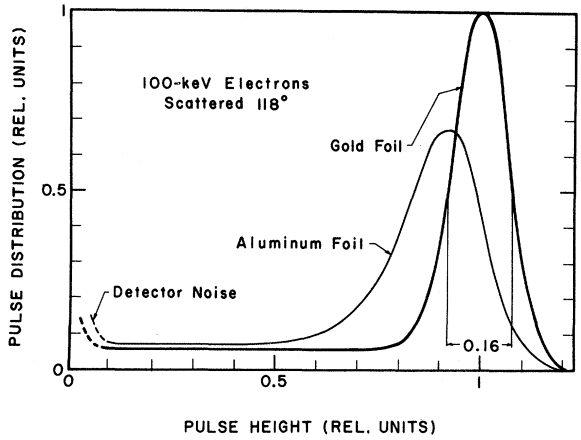

FIG. 20. Typical pulse-height spectra obtained with the solid-state detectors in the Mott-scattering chamber for scattering from a gold and an aluminum foil.

$$\rho_{Au} = (0.65 \pm 0.05)\rho_{Al} \qquad (3.9)$$

from the scattering of unpolarized electrons (originating at the copper-mesh photocathode in the ionizer (cf. Fig. 18) by the aluminum and gold foil for various angles of beam incidence. For the actual measurements beam steering was used to minimize the rotational asymmetry ρ_{Al} so that in no case did ρ_{Au} exceed $0.03 \times \delta_{Au}$.

Instead of scattering polarized electrons from aluminum to eliminate the rotational asymmetry, we could have scattered unpolarized "mesh" photoelectrons from gold. This, however, would have introduced an asymmetry originating from the different electron-optical conditions for the polarized and unpolarized beams, and hence additional measurements with an aluminum foil would have been necessary for a check of the two-beam asymmetry. Another approach to avoid the rotational asymmetry is not to rotate the scattering chamber at all. This would have necessitated reversal of the electron polarization by reversing the direction of the ionizer magnetic field, and would have led to changes in the electron optics and again to a new field-reversal asymmetry.

To eliminate the effects of multiple and plural scattering in the gold foil, the polarization asymmetries δ_{Au1} and δ_{Au2} were determined for two gold foils of different thicknesses t_1 and t_2, respectively. For the two foils used, the thickness ratio was $t_2/t_1 = 3.03$ ($\pm 1\%$). The gold foils were thin enough so that the relation

$$(1/\delta_t) = (1/\delta_0)(1 + \alpha t), \quad \alpha = \text{const} \qquad (3.10)$$

applied,[59] where δ_t is the polarization asymmetry for a foil of thickness t and δ_0 is the extrapolated value for $t \to 0$. The extrapolated asymmetry δ_0 was 26% higher $[(\delta_0 - \delta_t)/\delta_t = 0.26]$ than that measured with the thicker gold foil of 105 $\mu g/cm^2$. With the value of $S = 0.39 \pm 0.01$ for $\theta = 118°$ and $E = 100$ keV (cf. Fig. 5), α was then found to be 0.0035 $cm^2/\mu g$. The value of the electron polarization was calculated from the relation $P_e = \delta_0/S$.

4. *Background Corrections*

Before Eqs. (3.5)–(3.10) were used, the counts C_A and C_B were corrected for counts of inelastically scattered electrons. Typical smoothed pulse-height spectra for scattering from Au and Al foils are shown in Fig. 20. The subtraction of background was done by using a linear extrapolation of the nearly flat background. From measurements taken with a pure Formvar foil, it was found that scattering from the Formvar backing of the gold and aluminum foils is highly inelastic and contributed less than 0.1% of the elastic peaks in the spectra of Fig. 20.

A background which is difficult to eliminate is illustrated in Fig. 21. It may arise from the scattering of electrons by the foil in conjunction with scattering by the walls of the Mott scattering chamber. Since this background effect is proportional to the thickness of the foil, it cannot be eliminated by foil-thickness extrapolation or by a null-effect measurement with the foil removed. The effect was minimized by coating the walls with carbon, combined with pulse-height analysis. The remaining contribution is estimated to be less than 1%.

The case of the pulsed electron beam was more complicated, because the high instantaneous beam current resulted in a significant probability of detecting more than one electron per pulse. Those events appear in the pulse-height spectrum beyond the 100-keV peak. Hence for the polarization mea-

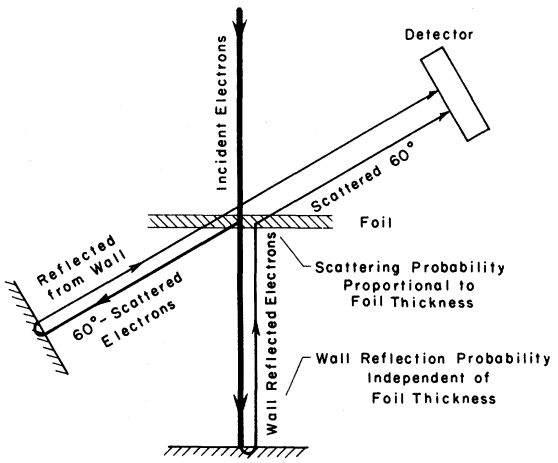

FIG. 21. Schematic illustration of a background effect in Mott scattering whose intensity is proportional to the thickness of the scattering foil.

surements with the pulsed electron beam, the current was reduced so that the detection of two scattered electrons in no case contributed more than 1% to the total number of counts in the spectrum.

IV. RESULTS

A. Electron Intensity

As will be seen in Sec. IV B, for the potassium photoionization, it was necessary that a light filter be inserted in order to obtain the expected electron polarization. With this filter in place we obtained an electron current of 1×10^{-12} A or 6×10^{6} electrons/sec. Since the measured potassium beam flux was 7×10^{13} atoms/sec, this corresponds to an ionization probability of about 10^{-7}. For continuous photoionization of lithium, without the use of a light filter, the electron current obtained was about 10^{-11} A or 6×10^{7} electrons/sec, corresponding to an ionization probability for the lithium beam atoms of about 2×10^{-7}. These dc electron currents are sufficiently large for measurements of the electron polarization.

Much higher photoelectron currents can be obtained by using a pulsed light source, since pulsed light sources such as sparks have a peak radiance in the ultraviolet which is many orders of magnitude larger than that of continuous lamps.[60] With the spark light source which was described in Sec. III B we obtained up to 2×10^{8} electrons/pulse. At a repetition rate of 10 sec^{-1} this is an average current of 3×10^{-10} A. The pulsed electron current obtained corresponds to an ionization probability of 2–3% for the lithium atoms in the ionization region. (Atom motion during the duration of the flash is negligible.) A fast electron detector consisting of an aluminum-covered plastic scintillator and a photomultiplier was used to observe the shape of the electron pulse. The electron pulses were 1–1.5 μsec long.

The spark light source was usually operated with argon at a pressure of 7 atm. Similar results were obtained with xenon. Nitrogen yielded a much lower intensity and a longer pulse; it also led to increased sputtering of electrode material. Helium also yielded a lower intensity. A study of the dependence of the electron intensity on the argon pressure in the spark chamber showed that a reduction of the pressure from 7 to 1 atm reduced the peak electron intensity by only a factor of $\frac{1}{2}$, while at the same time reducing the pulse length by a factor of $\frac{1}{2}$. This indicates that the spark plasma was at least partially opaque to the radiation at 7 atm.

From the measured electron and atomic beam intensities together with the lithium photoionization cross section, we estimate that the useful light (intersecting the atomic beam in the ionizing region and having wavelengths between the lithium threshold and the cutoff of Suprasil) corresponded to a radiant energy of approximately 1 mJ per flash. This value is in reasonable agreement with estimates for our light source and optical arrangement made on the basis of other investigations of spark discharges[60–65] which show that a light output corresponding to blackbody radiation of 35 000–40 000 °K is achievable.

The power supply used limited the repetition rate to 10 pulses/sec. Significantly higher repetition rates would also have required cooling of the spark source. The spark electrodes, made of tungsten with conical tips, had to be remachined occasionally since the spark caused sputtering of the metal. In addition, the window which sealed the high-pressure spark chamber had to be replaced when the vaporized metal, which condensed on the window, reduced the transmittance significantly. The pulse intensity fluctuated by as much as ± 50% because of changes in the spark position which, when magnified about four times by our optical system, led to changes in the atomic beam illumination.

Most studies of the pulsed beam were made with Suprasil windows and the optics chamber at atmospheric pressure. The use of LiF windows in conjunction with an evacuated optics chamber did not lead to an increase in the pulsed beam intensity. With LiF windows the useful wavelength range should have extended from the threshold at 2300 Å down to the LiF cutoff at 1050 Å. By comparison, the Suprasil cutoff lies at about 1700 Å. Thus, a corresponding intensity increase was expected. One possible explanation for the negative result is absorption at shorter wavelengths by oil films on the window.

B. Electron Polarization

1. *Depolarization Effects*

The predicted electron polarization for photoionization of polarized alkali atoms is given by $P_e = P_{at} = s f(H)$ if background electrons are avoided and if the photoionization does not affect the electron spin. Contamination of the electron beam by unpolarized photoelectrons originating at the electrode walls was effectively avoided by the electron-optical arrangement. There are, however, a number of nontrivial depolarization effects which can lead to a lower electron polarization in the extracted beam. Depolarization effects, discovered and studied in the potassium work, are photoionization of alkali molecules and photoionization of optically excited alkali atoms. The spin-orbit perturbation in the continuum P states of potassium was not detectable under the conditions of this experiment. In the case of lithium, the depolarization effects were found to be either negligible or avoidable.

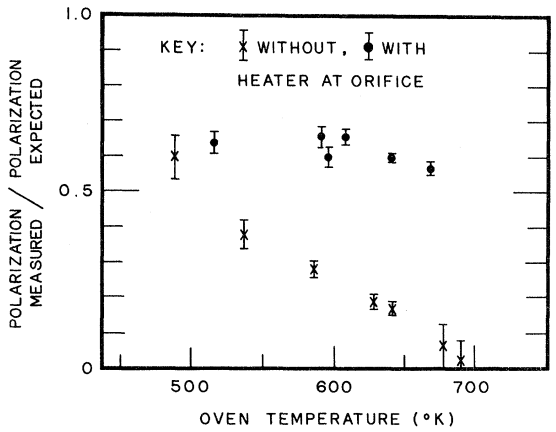

FIG. 22. Data on the polarization of electrons from photoionization of polarized potassium atoms, showing the depolarization effect related to the oven temperature (cross points). By means of overheating the oven orifice, this depolarization effect was eliminated (dot points). All data shown in this figure were obtained with scintillation detectors which did not have sufficient resolution to discriminate against electrons scattered from the walls of the Mott scattering chamber. (See Sec. II E 2.) The measured polarization increased by a factor of 1.28 when silicon surface barrier detectors were used.

2. *Photoionization of Alkali Molecules*

The discovery that photoionization of molecules can lead to substantial depolarization was made in the early potassium studies.[8] Measurement of the electron polarization at a potassium-oven temperature of 680 °K gave a value very close to zero. However, when the oven temperature was decreased, the electron polarization increased significantly, as shown by the data "without heater at orifice" of Fig. 22. The polarization was found to be independent of transverse oven position, thus proving that the effect was not due to a temperature-dependent oven misalignment. Later a study of the alkali-molecule problem revealed that even a very small K_2 contamination of the atomic beam can contribute a large portion of the photoelectrons and that the ratio of molecules to atom does indeed increase with oven temperature.

In thermodynamic equilibrium the molecule to atom ratio is given by[66]

$$\gamma = 4hR^2N_0\left(\frac{\pi}{mkT}\right)^{1/2}\frac{273}{T}\,\frac{p}{760}\,e^{U_0/kT}, \qquad (4.1)$$

where R is the radius of gyration of the molecules in Å, N_0 Avogadro's number, T the temperature in °K, p the pressure of the vapor in Torr, U_0 the dissociation energy of the molecule, h Planck's constant, m the mass of the atom, and k Boltzmann's constant. The pressure p of saturated alkali vapor can be described by

$$\ln p = A - B/T, \qquad (4.2)$$

where A and B are constants, and hence

$$\gamma = (\text{const}) \times T^{-3/2}\,e^{(U_0 - Bk)/kT}. \qquad (4.3)$$

For potassium, $U_0 = 0.514$ eV[67] and $B = 4480$ °K,[68] so that $U_0 - Bk = -0.165$ eV. Since the exponent in Eq. (4.3) is negative and the exponential term dominates the temperature dependence of γ up to 2900 °K, the molecule to atom ratio increases with increasing temperature in the range over which the oven temperature was varied. In order to calculate γ we evaluated the constant in Eq. (4.3) using $R \simeq 1.95$ Å[69] and $A = 1.028 \times 10^{-2}$ Torr.[68] We obtained $\gamma = 0.002$ for $T = 620$ °K. The ratio in the beam was somewhat smaller because molecules were not focused by the six-pole magnet.

The photoionization cross section of K_2 is about 1 Mb in the region of $\lambda = 2500$–2900 Å, whereas the cross section of K is only 0.1 Mb near threshold and close to zero in the cross-section minimum near 2720 Å.[31] Furthermore, the ionization potential of K_2 is at least 0.24 V smaller than that of K, as inferred from data of Lee and Mahan.[70] Since unfiltered light from a mercury high-pressure arc lamp was originally used in our experiment, the light beam contained many photons with energies in the range below the threshold of atomic ionization but above that of molecular ionization. The ground state of the potassium molecule is a $^1\Sigma$ state with zero spin. Therefore, photoelectrons from K_2 are unpolarized. If all these factors are taken into account, the depolarization effect due to K_2 molecules, as exhibited in Fig. 22, can be explained.

Avoidance of this K_2 depolarization effect can be achieved through the use of an atomic beam emerging from an unsaturated vapor. In other words, the vapor near the oven orifice has to have higher temperature and/or a lower pressure than the vapor which is in equilibrium with the metal reservoir. This condition was achieved with an extra heater attached to the oven orifice. The consequent temperature increase of several hundred degrees eliminated the temperature dependence of the photoelectron polarization, as shown by the points "with heater at orifice" of Fig. 22.

For lithium, the depolarization due to molecule photoionization is less serious because atomic and molecular photoionization cross sections are of the same magnitude.[71] Nevertheless, the lithium oven was designed to have the orifice at higher temperature and lower pressure than the metal reservoir.

3. *Photoionization of Optically Excited Atoms*

Elimination of the molecules from the atomic beam did not yield agreement between measured

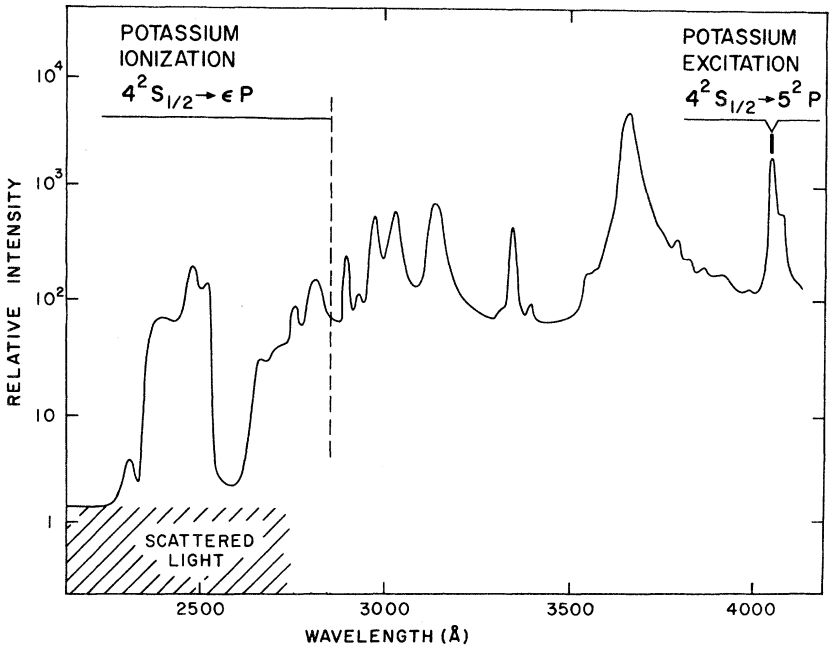

FIG. 23. Spectrum of the Osram HBO 200W/2 mercury lamp in which the location of the atomic ionization threshold and the wavelength of the 4S-5P transition of potassium are indicated. The spectrum was measured with a 0.3-m scanning monochromator set for 13-Å resolution. The use of a phototube with S1 spectral sensitivity coated with sodium salicylate resulted in a flat spectral response to within 1.0% from 1000 to 3500 Å.

and expected polarization (cf. Fig. 22). It was discovered that an electron current as large as 12% of the total current was obtained with the atomic beam on and with a sheet of window glass or acrylic plastic in front of the quartz window which allowed only wavelengths longer than 3200 Å to enter the ionization region. No current should have occurred under this condition since the light did not have sufficient energy to photoionize ground-state atoms (ionization threshold equal to 2856 Å). Furthermore, it was found that these electrons had a polarization smaller than that measured without light filters by a factor 0.72 ± 0.05. Hence these anomalous electrons could not be photoelectrons from surfaces, which would have been unpolarized. Impurities in the technical grade potassium metal such as Rb could not be responsible for these anomalous electrons, because the effect remained when highly pure potassium metal was used in the oven. Collisional ionization of potassium atoms, optically excited to high nP states, was ruled out by studies at different beam densities and residual gas pressures.

The mechanism responsible involves photoionization of potassium atoms which have been excited to lower P states by the longer-wavelength light from the lamp. Since this process requires two photons, the anomalous electron current should have changed quadratically with light intensity. This was established by the use of pieces of window screen that had an open area of 50% which reduced light intensity by factors of 2 without affecting the optical geometry or spectral distribution. The fraction of the current produced by unfiltered light which exhibited the quadratic behavior was found to be 0.32 ± 0.03.

The reason for this large contribution is a coincidence of an intense line of the mercury arc spectrum near 4050 Å and the $4^2S_{1/2} - 5^2P$ resonance line of potassium (Fig. 23). The fact that the electrons originating from the 5^2P state are polarized, although somewhat less than those originating from the ground state, can be understood from Fig. 24. To estimate this effect we assume that the nuclear spin is decoupled and that the ground-state atoms are completely polarized, oc-

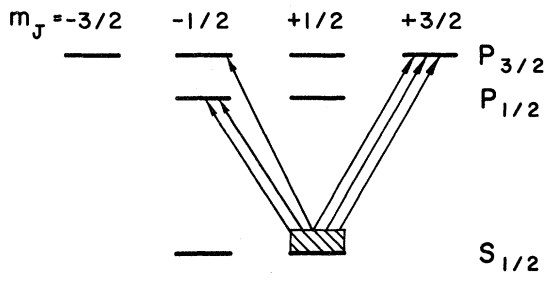

FIG. 24. Schematic illustration of atomic excitation (nuclear spin decoupled). The ground-state atoms are assumed to be in state $m_J = +\frac{1}{2}$. Unpolarized light incident parallel to the magnetic field induces the transitions indicated by the arrows. The number of arrows gives the relative strengths of these transitions.

cupying the $m_J = +\frac{1}{2}$ state. Unpolarized light incident parallel to the magnetic field can only induce transitions with $\Delta m_J = \pm 1$. For a spectral flux from the lamp which is constant over the small-wavelength interval between the $P_{3/2}$-$P_{1/2}$ line doublet, the relative strengths of the optical transitions are indicated by the number of arrows in Fig. 24. For unity polarization of the ground-state atoms, the average electronic polarization of the excited atoms is calculated to be $\frac{7}{12} = 0.583$. If the ground-state atomic polarization is less than unity, as in the potassium experiment where $P_{at} = sf(H) = 0.57$, the polarization of the excited atoms should be $0.57 \times 0.583 = 0.332$. If 32% of the electrons result from ionization of excited atoms and the remaining 68% from ionization of ground-state atoms, the net electron polarization should be $0.32 \times 0.332 + 0.68 \times 0.57 = 0.494$. Elimination of the photoelectrons from excited atoms should then lead to an increase of the electron polarization by the factor $0.57/0.494 = 1.15$. We eliminated these photoelectrons by use of an appropriate filter (see below), and we measured an increase of the electron polarization by the factor 1.19 ± 0.04, in good agreement with the explanation given above. (Agreement between measured and expected values of the electron polarization was achieved after improvements in the Mott-scattering electron detection were implemented, which increased the measured electron polarization by another factor of 1.28.)

Elimination of this effect was achieved with the use of a filter consisting of a $NiSO_4$ solution in a quartz tank. With the thickness of 1 cm, the filter transmitted about 90% of the radiation between 2400 and 3100 Å and none at 4050 Å.[72]

For the work with lithium the wavelengths of the Li resonance lines were checked against the lines in the xenon-mercury arc spectrum and the significant argon atomic and ionic lines in the spark spectrum. No such coincidence was found. However, since the two-step photoionization process depends quadratically on the light intensity and since the instantaneous intensity in the spectral continuum of the pulsed light source may be very high, it was necessary that the electron polarization be measured as a function of the light intensity. Such measurements showed that the two-step photoionization process did not contribute significantly in pulsed photoionization of lithium.

4. *Spin-Orbit Perturbation*

As mentioned in Sec. III C, for photoionization with unpolarized light the polarization of the photoelectron P_e is related to the electronic polarization of the atom P_{at} by $P_e = R\,P_{at}$ with $R = X^2/(X^2+2)$, where X is the wavelength-dependent perturbation function which has been determined in experiments involving photoionization of polarized alkali atoms with circularly polarized photons.[7] For potassium, the depolarization parameter R as a function of photon wavelength has the form shown in Fig. 25. It can be seen that depolarization is significant only in a small-wavelength interval around $\lambda = 2720$ Å. In order to determine the effective depolarization, $R(\lambda)$ must be considered in conjunction with the cross section, $\sigma(\lambda)$, and the spectral distribution of the light source.

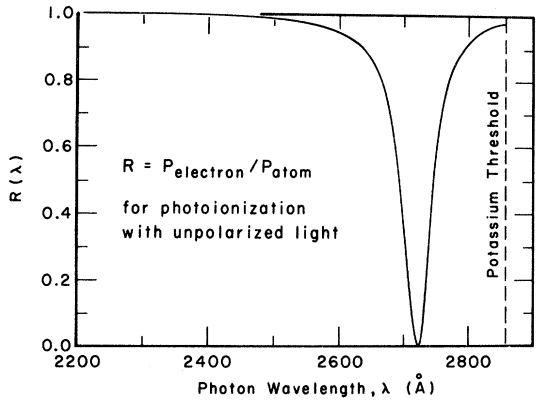

FIG. 25. Depolarization parameter R as a function of light wavelength for photoionization of polarized potassium atoms by unpolarized light. This function was calculated from the experimental results on spin-orbit perturbation in potassium (Refs. 7 and 33).

The photon distribution of the light source $\Phi(\lambda)$ was obtained from the spectral energy distribution of Fig. 23 and is plotted in Fig. 26(a). For the potassium cross section we used an upper limit which was derived from the perturbation data[7,33,73] which gives a minimum of only 2% of the threshold cross section, in good agreement with Seaton's theoretical estimate[32] and consistent with the data of Hudson and Carter[31] but much lower than that of Marr and Creek[30] (Fig. 3). The number of photoelectrons produced is proportional to $\int \Phi(\lambda)\sigma(\lambda)\,d\lambda$, as illustrated by the hatched area of Fig. 26(b). Finally, the number of unpolarized electrons produced is proportional to $\int \Phi(\lambda)\sigma(\lambda)[1 - R(\lambda)]\,d\lambda$ as shown by the hatched area of Fig. 26(c). Note that the hatched areas in both figures are roughly equal in size. However, the scale in Fig. 26(c) is enlarged by the factor 100. The depolarization thus estimated amounts to about 1% and was not detectable in our polarization measurement where the accuracy was only 6%.

In lithium the depolarization due to spin-orbit perturbation is negligibly small for two reasons. First, the perturbation is a relativistic effect which decreases with the atomic number Z of the alkali atoms. Second, the resulting depolarization is only significant in the vicinity of a cross-section minimum. Lithium does not exhibit such a mini-

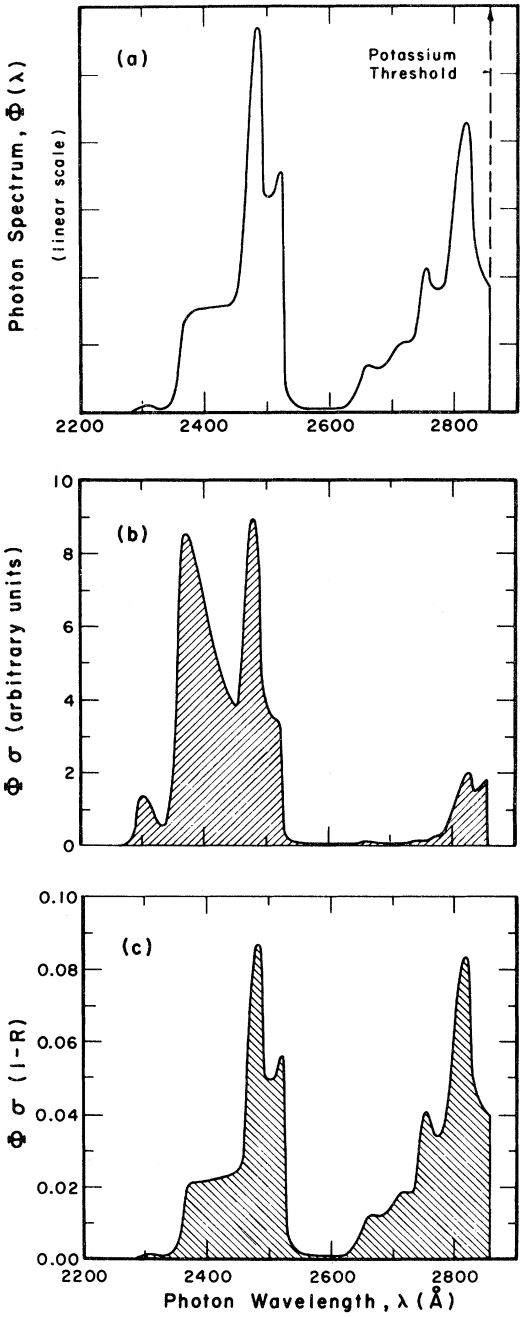

FIG. 26. Plots for estimating the depolarization due to spin-orbit perturbation in the potassium photoionization experiment. Plot (a) represents the photon distribution of the light source. The hatched area in plot (b) corresponds to the total number of electrons produced while the hatched area in plot (c)—scaled up by a factor of 100—corresponds to the number of electrons which were depolarized.

mum (Fig. 3).

5. *Final Polarization Results*

The final electron polarization for potassium obtained after elimination of the depolarization effects discussed above was $P_e = 0.58 \pm 0.03$,[8] as compared with an expected electron polarization of 0.57 based on the calculated values of $f(H) = 0.58$ for a field of 90 G and a state-selection parameter of $s = 0.98$.

For lithium the data on the electron polarization are shown in Fig. 27. The vertical error bars correspond to 1 standard deviation. The error resulting from counting statistics is approximately $\pm 1.5\%$. The remainder of the error results from uncertainties in the foil thickness extrapolation and knowledge of the function S [cf. Eq. (3.10)]. The horizontal error bar is based upon the variation of the magnetic field over the region in which the atomic beam was photoionized. The theoretical electron polarization was calculated for a beam of the isotopic composition 95.6% Li^6 and 4.4% Li^7, and a state-selection parameter of $s = 0.96$.

Within the accuracy of the data, the results agree with the expectation. Any remaining depolarization is certainly less than 3% and was too small to be investigated systematically. Both photoionization of Li_2 molecules and spin-rotation during extraction from the magnetic field of the ionizer could perhaps have contributed depolarizations on the order of 1%.

C. Pulsed Photoionization of Polarized Lithium Atoms as a Source of Polarized Electrons

Polarized electron beams are useful for other physics research. Several methods of obtaining polarized electrons are known, but no single source is ideal for all kinds of polarization experiments.[74] The pulsed photoionization of polarized lithium atoms which we have investigated appears to be particularly useful for providing a source of

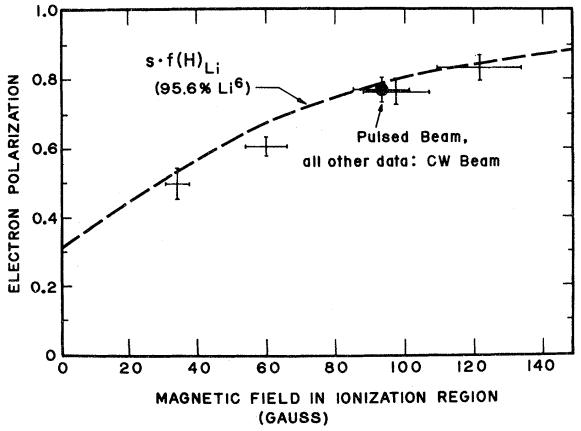

FIG. 27. Results of the electron polarization measurements in the experiment on photoionization of polarized lithium atoms. The metal used was 95.6% Li^6 and 4.4% Li^7. The dashed curve $sf(H)$ describes the calculated electronic polarization of the atoms.

polarized electrons for injection into a pulsed high-energy accelerator.[9,75] The pertinent data of our source are compared with the published data of other sources in Table II.

Some improvement in the peak current is possible through the use of a multi-channel oven[49] or a jet atomic beam source.[94] The repetition rate can certainly be increased by technical improvements on the spark light source[95] and the associated electronics. An electron polarization up to 90% is achievable by using a stronger magnetic field in the ionizer of about 200 G. The accompanying increase in emittance (skew parameter) can be tolerated for accelerator injection.[75]

ACKNOWLEDGMENTS

The IBM Thomas J. Watson Research Laboratories kindly provided some of the components for the polarization converter and Mott scattering chamber. We gratefully acknowledge the valuable assistance provided by the technical staff of Gibbs Laboratory including A. Disco, D. Constantino, and D. Moler. We also wish to thank M. Ratner for making the gold foils and J. Shore and J. Ladish for their help with the computer calculations. We especially wish to express our appreciation for the valuable discussions which we had with Dr. G. Baum during the preparation of this manuscript.

APPENDIX A: STATE-SELECTION PROPERTIES OF SIX-POLE MAGNET

The magnetic field H inside an ideal six-pole magnet is proportional to the square of the radial distance r from the axis; that is,

$$H(r) = r^2(H_R/R^2) , \tag{A1}$$

where R is the magnet gap radius and H_R is the field at the pole tips. The force acting on the atomic magnetic moment is given by

$$\vec{F}(r) = \mp \mu_0 \vec{\nabla} H = \mp (2\mu H_R/R^2)\vec{r} \tag{A2}$$

in the strong-field limit where the magnetic moment μ is independent of the field H. For ground-state alkali atoms whose nuclear spin is decoupled from the electronic angular momentum, the upper sign refers to atoms in the Zeeman state with $m_J = +\frac{1}{2}$ and the lower sign, to $m_J = -\frac{1}{2}$. The assumption of decoupling is only valid in strong magnetic fields where μH is larger than or, at least, of the order of the hyperfine-structure (hfs) interaction energy. This is certainly not valid in regions very close to $r = 0$ where the magnetic field approaches zero. On the other hand, in the region close to the axis, the force acting on the dipole moment is also very small. Since the trajectory of the atom is affected predominantly in the high-field region of the magnet, use of Eq. (A2) is a good approximation.

We will use a coordinate system with the z axis along the axis of the magnet and $z = 0$ at the magnet entrance. Since the force is radial and depends only on the radius r, the equations of motion are the same for the x and the y components. We will write only the equations for x, unless different initial conditions in x and y are considered. First we assume that the atoms come from a point source on axis and hence $x_s = 0$ and $y_s = 0$. Off-axis source points and the resulting vignetting are discussed later.

From Eq. (A2) it follows that

$$\frac{d^2x}{dt^2} \pm \omega^2 x = 0 , \tag{A3}$$

where $\omega = (2\mu_0 H_R/mR^2)^{1/2}$ and m is the atomic mass. Thus atoms with $m_J = +\frac{1}{2}$ [upper sign in Eq. (A3)] traverse the magnet on a sinusoidal trajectory whereas atoms with $m_J = -\frac{1}{2}$ are deflected from the axis on a hyperbolic trajectory [lower sign of Eq. (A3)]. For atoms in the state $m_J = +\frac{1}{2}$ we obtain

$$x_+(t) = \left(\frac{dx}{dt}\right)_0 \frac{1}{\omega} \sin\omega t + x_0 \cos\omega t \tag{A4}$$

and

$$x_+(z) = \left(\frac{dx}{dz}\right)_0 \frac{v}{\omega} \sin(\omega z/v) + x_0 \cos(\omega z/v) , \tag{A5}$$

where v is the atom velocity and

$$\frac{dz}{dt} = v_z \simeq v . \tag{A6}$$

As in Sec. III A we will use the inverse-velocity parameter

$$\eta = (1/v)(4kT/m)^{1/2} \tag{A7}$$

as well as the source-to-magnet entrance distance A, magnet length L, magnet gap radius R, source radius R_s, source temperature T, magnet pole-tip field H_R and the two distribution functions $F_{\mathrm{GAS}}(\eta)$ and $F_{\mathrm{BEAM}}(\eta)$ plotted in Fig. 9. The various formulas take on a simplified form with the use of the following three dimensionless constants:

$$K = (\mu_0 H_R/2kT)^{1/2} , \quad C_1 = KA/R , \quad C_2 = KL/R . \tag{A8}$$

For the experimental conditions in our lithium experiment these constants had the values $K = 0.0172$, $C_1 = 0.791$ and $C_2 = 1.926$. We can rewrite Eq. (A5) in terms of K, C_1, and C_2 as

$$x_+(z) = \left(\frac{dx}{dz}\right)_0 \frac{R}{\eta K} \sin\left(\eta C_2 \frac{z}{L}\right) + x_0 \cos\left(\eta C_2 \frac{z}{L}\right) , \tag{A9}$$

where

$$\left(\frac{dx}{dz}\right)_0 = x_0' = \frac{x_0}{A} \tag{A10}$$

TABLE II. Comparison of existing polarized electron sources.

Method	Group	Average current (electrons/sec)	Mode	Peak current[a] 1.5 μsec pulse (electrons/pulse)	Polarization	Beam characteristics (where available)
Mott scattering						
Au, 161 keV	Groningen[76]	2×10^{9}	dc	3×10^{3}	20%	Emittance 6 mrad cm at 161 keV
Hg, 300 eV	Mainz[77]	6×10^{9}	dc	9×10^{3}	17%	
Hg, 900 eV	Mainz[78]	6×10^{6}	dc	10	53%	
Hg, 900 eV	Karlsruhe[79]	6×10^{5}	dc	1	84%	
Hg, 6.75 eV	Mainz[80]	10^{11}	dc	1.5×10^{5}	27%	
Au solid, 32 keV	Berlin[81]	3×10^{7}	dc	45	27%	
Spin exchange						
Polarized K atoms	Edinburgh[82]	2.5×10^{7}	pulsed	6×10^{4}	10%	Repetition rate 100–2000 pulses/sec [b] Pulse length 1 μsec
Field emission						
Magnetized Gd	Munich[83,84]	...[c]	pulsed	...	8%	Extraction from pulsed 10-kG field
Photoemission						
Magnetized Gd	Zurich[85]	...	dc	...	5%	Extraction from 14-kG field
Magnetized EuO	Zurich[86]	...	dc	...	17%	Extraction from 7.5-kG field
Magnetized EuSe	Zurich[86]	...	dc	...	22%	Extraction from 14.5-kG field
Magnetized EuS	Zurich[87]	...	dc	...	53%	Extraction from 30-kG field. Quantum yield 10^{-4} electrons/5 eV photon
Magnetized Ni	Zurich[88]	...	dc	...	15%	Extraction from 10-kG field
Magnetized Co	Zurich[89]	...	dc	...	21%	Extraction from 17-kG field. Quantum yield 2×10^{-4} electrons/5.5 eV photon
Magnetized Fe	Zurich[89]	...	dc	...	54%	Extraction from 30-kG field
Optical pumping						
He discharge	Rice[90]	2.5×10^{13}	dc	4×10^{7}	8%[d]	Extraction from 5-G field
Fano effect						
Cs	Karlsruhe[91]	2×10^{8}	dc	3×10^{2}	81%	
	Yale[33,73]	10^{10}	dc	1.5×10^{4}	65%	3 mrad cm at 2 keV
Photoionization						
Polarized K atoms	Yale[8]	6×10^{6}	dc	10	58%	
	Orsay[92]	1.5×10^{7}	dc	23	45%[e]	
	Bonn[93]	10^{9}	pulsed	2×10^{6}	55%	Emittance 2 mrad cm at 120 keV Repetition rate 50 pulses/sec. Pulse length 15 μsec
Polarized Li^{6} atoms	Yale, this work	2×10^{9}	pulsed	2×10^{8}	78%	Emittance 1 mrad cm at 100 keV. Repetition rate 10 pulses/sec. Pulse length 1.5 μsec

[a]For dc sources the peak current represents the current of a chopped beam during 1.5 μsec.

[b]The Edinburgh group cites an average current of 4×10^{-12} A and a peak intensity of 10^{-8} for a 1 μsec pulse. These correspond to the values given in the table. It should be noted that these values correspond to a repetition rate of 400 pulses/sec, not the 100 pulses/sec quoted in the Edinburgh paper.

[c]The Munich group cites an average current of 6×10^{10}–6×10^{11} electrons/sec in a dc mode with magnetic field turned off. The magnetic field was pulsed on for 130-μsec intervals.

[d]A polarization as high as 17% was observed furing the 100-μsec afterglow of the discharge.

[e]Although the Orsay paper claims a polarization of 90%, we believe that based upon the raw data presented, this figure is incorrect and should be 45% as listed above.

for a point source on axis. The derivative of Eq. (A9) is

$$\frac{dx_+(z)}{dz} = x_0' \cos\left(\eta C_2 \frac{z}{L}\right) - \frac{x_0}{R}\eta K \sin\left(\eta C_2 \frac{z}{L}\right) . \quad \text{(A11)}$$

If $dx_+(z)/dz = 0$ for $0 < z < L$, the maximum value of $x(z)$ for the trajectory occurs inside the magnet. Let η^* be the value for which $x = x_{max}$ at $z = L$. From Eqs. (A9) and (A11) it follows that η^* is determined by

$$x_0' \cos(\eta^* C_2) - (x_0/R)\eta^* K \sin(\eta^* C_2) = 0$$

or

$$\cot(\eta^* C_2) = \eta^* C_1 . \quad \text{(A12)}$$

The solid angle which describes the transmittance of the magnet can be defined as

$$\Omega^+(\eta) = \pi[x_{0,\max}(\eta)]^2/A^2 . \quad \text{(A13)}$$

The maximum entrance coordinate for a trajectory with $x \leq R$ throughout the magnet can be found from Eq. (A9). For $\eta < \eta^*$ we require that $x_+(L) \leq R$ and find

$$x_{0,\max}(\eta) = \frac{A\eta K}{\sin(\eta C_2) + \eta C_1 \cos(\eta C_2)} . \quad \text{(A14)}$$

For $\eta > \eta^*$ we require that the amplitude of the sinusoidal trajectory

$$x = [(x_0/\eta C_1)^2 + x_0^2]^{1/2} \quad \text{(A15)}$$

not exceed R. Then we find

$$x_{0,\max}(\eta) = A\eta K/[1 + (\eta C_1)^2]^{1/2} . \quad \text{(A16)}$$

Combining Eqs. (A13)–(A16) we obtain

$$\Omega^+(\eta) = \pi(\eta K)^2/[\sin(\eta C_2) + \eta C_1 \cos(\eta C_2)]^2 \quad \text{for } \eta \leq \eta^* \quad \text{(A17a)}$$

and

$$\Omega^+(\eta) = \pi(\eta K)^2/[1 + (\eta C_1)^2] \quad \text{for } \eta \geq \eta^* , \quad \text{(A17b)}$$

with η^* determined by Eq. (A12).

The values of $\eta < \eta^*$ correspond to the very fast atoms whose trajectories are still diverging at the magnet exit. The trajectories for atoms with $\eta > \eta^*$ bend toward the axis inside the magnet at radial distances $\leq R$. Therefore, the second expression for Ω^+ is independent of the magnet length, contained in C_2. For our parameter values we find $\eta^* = 0.59$; thus, it is the second expression for Ω^+ which dominates (cf. Fig. 9). Note that Ω^+ depends strongly on H_R, contained in the constant K, but not very much on the ratio A/R, contained in the constant C_1 (since $C_1^2 = 0.62 < 1$). For atoms in the state $m_J = -\frac{1}{2}$, a similar calculation gives

$$\Omega^-(\eta) = \pi(\eta K)^2/[\sinh(\eta C_2) + \eta C_1 \cosh(\eta C_2)]^2 . \quad \text{(A18)}$$

Both functions, Ω^+ and Ω^-, are plotted in Fig. 10 for the parameter values of our experiment.

The trajectory slope at the magnet exit follows from Eq. (A11) and accordingly is given by

$$\alpha_{exit} = \left(\frac{dx_+}{dz}\right)_{z=L} = (x_0/A)\cos(\eta C_2) - x_0(\eta K/R)\sin(\eta C_2) . \quad \text{(A19)}$$

The maximum value of $|\alpha_{exit}|$ is obtained when $x_0 = R$:

$$|\alpha_{exit}|_{max} = \eta K|\sin(\eta C_2) - (1/\eta C_1)\cos(\eta C_2)| . \quad \text{(A20)}$$

With our parameter values $C_1 \simeq 0.8$ and $C_2 \simeq 1.9$ we can approximate $\sin(\eta C_2) \simeq 1$, $\cos(\eta C_2) \simeq 0$ for the η values near unity. For the purpose of this estimate we can use $\eta = 1$, which corresponds to the peak of the distribution function F_{GAS}. Thus we obtain $|\alpha_{exit}| < K$. Along the axial distance $D \simeq 14$ cm between the magnet exit and the ionizer, the atomic beam diverges in the radial direction by not more than $KD = 0.24$ cm. Since this radial distance is of the same order as the magnet gap radius ($R = 0.16$ cm) as well as the size of the light source image in the ionizer, more detailed calculations for the beam profile at the ionizer are not necessary in our case. We therefore chose the magnet length on the basis of the state-selection parameter desired (cf. Fig. 11) rather than on the basis of its focusing properties. The magnet gap radius was chosen as 0.16 cm because such a radius is large enough to permit accurate machining at reasonable cost, but it is still small enough to provide a large value for L/R, which ensures good state selection, without going to an unwieldy magnet length L. A treatment of the focusing properties of six-pole magnets was recently given by Brash *et al.*[96]

APPENDIX B: VIGNETTING CALCULATIONS FOR EXTENDED SOURCES

We derived the transmittance solid angles of Eqs. (A17) and (A18) for a point source on axis. The decrease of transmittance for increasing radial distance of the source point is called vignetting by analogy to light optics.[97] In order to estimate the effect of vignetting, we consider a source point off axis, at $x_s \neq 0$, $y_s \neq 0$. The trajectory inside the magnet, given by Eq. (A9), can be rewritten as

$$x_+(z) = a \sin[\eta(K/R)z] + b \cos[(\eta K/R)z] , \quad \text{(B1)}$$

with

$$a = (x_0 - x_s)/\eta C_1 \text{ and } b = x_0 ,$$

The maximum of x_+ inside the magnet is

$$x_{max} = (a^2 + b^2)^{1/2} = \left[\left(\frac{x_0 - x_s}{\eta C_1}\right)^2 + x_0^2\right]^{1/2} . \quad \text{(B2)}$$

A similar equation holds for y. The radial distance

inside the magnet is

$$r(z)=[x(z)^2+y(z)^2]^{1/2}\ . \tag{B3}$$

As an approximation, we consider the case in which x and y go through maxima at the same value of z, that is,

$$r(z)=(x_{\max}^2+y_{\max}^2)^{1/2}\leq R\ . \tag{B4}$$

We use this to obtain an estimate on the intensity loss due to vignetting. From Eqs. (B2)–(B4) it follows that

$$R^2\geq\left(\frac{x_0-x_s}{\eta C_1}\right)^2+x_0^2+\left(\frac{y_0-y_s}{\eta C_1}\right)^2+y_0^2$$

$$=\frac{1}{(\eta C_1)^2}\left[(x_0-x_s)^2+(y_0-y_s)^2+x_0^2\right]+y_0^2\ . \tag{B5}$$

By substituting

$$x_0=x^*+\frac{x_s}{1+(\eta C_1)^2}\ ,\quad y_0=y^*+\frac{y_s}{1+(\eta C_1)^2} \tag{B6}$$

and going through some lengthy algebra, we obtain finally

$$R^2\geq\left(1+\frac{1}{(\eta C_1)^2}\right)(x^{*2}+y^{*2})+\frac{1}{1+(\eta C_1)^2}\ (x_s^2+y_s^2)\ . \tag{B7}$$

Now, we introduce a source-point radius $r_s=(x_s^2+y_s^2)^{1/2}$ and an aperture radius r_a, defined as $(x^{*2}+y^{*2})^{1/2}$ for the maximum value permitted by Eq. (B7). Then we obtain

$$R^2=\left(1+\frac{1}{(\eta C_1)^2}\right)r_a^2+\frac{r_s^2}{1+(\eta C_1)^2} \tag{B8}$$

and

$$r_a^2=R^2\left[1-\frac{(r_s/R)^2}{1+(\eta C_1)^2}\right]\left[\frac{(\eta C_1)^2}{1+(\eta C_1)^2}\right]\ . \tag{B9}$$

The source point at r_s has a transmittance solid angle

$$\Omega^+(r_s)=\frac{\pi r_a^2}{A^2}=\frac{\pi R^2}{A^2}\left(\frac{(\eta C_1)^2}{1+(\eta C_1)^2}\right)\left(1-\frac{(r_s/R)^2}{1+(\eta C_1)^2}\right)$$

$$=\left[\frac{\pi(\eta K)^2}{1+(\eta C_1)^2}\right]\left[1-\frac{(r_s/R)^2}{1+(\eta C_1)^2}\right]\ , \tag{B10}$$

where the first bracket equals $\Omega^+(r=0)$ as given by Eq. (A17b). The approximate vignetting condition of Eq. (B4) leads to the result that atoms originating at off-axis source points are transmitted by the magnet if they enter the magnet within a circular area which has its center at

$$x=\frac{x_s}{1+(\eta C_1)^2}\ ,\quad y=\frac{y_s}{1+(\eta C_1)^2}$$

and has a radius smaller than that for the on-axis source point by a factor of

$$\left(\frac{1-(r_s/R)^2}{1+\eta^2C_1^2}\right)^{1/2}$$

[cf. Eqs. (B6) and (B7)].

We therefore find for the average transmittance solid angle for a circular source orifice of radius R_s with $R_s\leq R$ the following expression:

$$\overline{\Omega}^+=\frac{1}{\pi R_s^2}\int_0^{R_s}\Omega^+(r_s)2\pi r_s\,dr_s$$

$$=\frac{2}{R_s^2}\Omega^+(0)\int_0^{R_s}r_s\left(1-\frac{(r_s/R)^2}{1+(\eta C_1)^2}\right)dr_s \tag{B11}$$

$$=\Omega^+(0)\left[1-\frac{1}{2}\,\frac{(R_s/R)^2}{1+(\eta C_1)^2}\right] \tag{B12}$$

$$=\Omega^+(0)\,C_{\rm vig}\ ,$$

where

$$C_{\rm vig}=1-\frac{1}{2}\,\frac{(R_s/R)^2}{1+(\eta C_1)^2}\ . \tag{B13}$$

Since most of the atoms transmitted lie in the vicinity of $\eta=1$, we can omit the factor η. For atoms in the state $m_J=-\frac{1}{2}$, the vignetting effect is negligible so long as $R_s\leq R$. This can be shown from the trajectory equation $x_-(z)$ for $R_s>0$ and the requirement that $x_-<R$ for $0\leq x\leq L$.

Note that the approximation made in this calculation [based on Eq. (B4)] overestimates the vignetting effect, thus giving a lower bound for $C_{\rm vig}$. In our case, we find $C_{\rm vig}=0.92$. Vignetting, in our case, thus has a negligible effect on the state-selection parameter. (The solid curve of Fig. 11 gives $s=0.960$ for the lithium experiment. This value is reduced to 0.956 by vignetting.)

*Work supported in part by the United States Office of Naval Research, under Contract Nos. NONR 609(53) and N00014-67-A-0097-0015, and the Air Force Office of Scientific Research, under Contract No. F44620-71-C-0042.

†Present address: Sandia Corporation, Albuquerque, N.M.

‡Present address: Department of Physics, University of Massachusetts at Boston, Boston, Mass.

[1]E. Fues and H. Hellmann, Physik. Z. 31, 465 (1930).

[2]H. Friedmann, Sitzber. Math. Naturw. Kl. Bayr. Akad. Wiss. München 3, 13 (1961).

[3]R. L. Long, Jr., W. Raith, and V. W. Hughes, Bull. Am. Phys. Soc. 10, 28 (1965).

[4]F. Bopp, D. Maison, G. Regenfus, and H. C. Siegmann, Z. Physik 185, 48 (1965).

[5]U. Fano, Phys. Rev. 178, 131 (1969); 184, 250 (1969).

[6]M. S. Lubell and W. Raith, Phys. Rev. Letters 23, 211 (1969).

[7]G. Baum, M. S. Lubell, and W. Raith, Phys. Rev. Letters 25, 267 (1970).

[8]R. L. Long, Jr., W. Raith, and V. W. Hughes, Phys. Rev. Letters 15, 1 (1965).

[9]V. W. Hughes, M. S. Lubell, M. Posner, and W. Raith, in *Proceedings of the Sixth International Conference on High Energy Accelerators, Cambridge, Mass.*

(Cambridge Electron Accelerator Laboratory, Cambridge, Mass. 1967), p. A144.

[10]P. G. Burke and H. M. Schey, Phys. Rev. 126, 163 (1962).

[11]W. Raith, in *Atomic Physics*, edited by V. W. Hughes, B. Bederson, V. W. Cohen, and F. M. J. Pichanick (Plenum, New York, 1969), p. 389.

[12]B. Bederson, Comments At. Mol. Phys. 1, 41 (1969); 1, 65 (1969); Phys. Today 22 (No. 11), 87 (1969).

[13]A. I. Akhiezer, L. N. Rozentsveig, and I. M. Shmushkevich, Zh. Eksperim. i Teor. Fiz. 33, 765 (1957) [Sov. Phys. JETP 6, 588 (1958)].

[14]V. W. Hughes, in *Proceedings of the Fifth Intenational Conference on High Energy Accelerators* (Comitato Nazionale per l'energia Nucleare, Rome, Italy, 1966), p. 531.

[15]J. D. Bjorken and E. A. Paschos, Phys. Rev. 185, 1975 (1969); S. D. Drell, D. J. Levy, and Tung-Mow Yau Yau, Phys. Rev. Letters 22, 744 (1969); H. Harari, *ibid.* 22, 1078 (1969); N. Dombey, Rev. Mod. Phys. 41, 236 (1969).

[16]J. D. Bjorken, Phys. Rev. D 1, 1376 (1970).

[17]L. Galfi, J. Kuti, and A. Patkos, Phys. Letters 31B, 465 (1970).

[18]G. Domokos, S. Kovesi-Domokos, and E. Schonberg, Phys. Rev. D 3, 1191 (1971).

[19]J. Kuti (unpublished).

[20]V. W. Hughes, R. L. Long, Jr., and W. Raith, in *Proceedings of the International Conference on High Energy Accelerators, Dubna, U.S.S.R.*, 1963, edited by Y. A. Smorodinsky (Atomizdat, Moscow, U.S.S.R., 1964), p. 988.

[21]W. Raith, R. L. Long, Jr., V. W. Hughes, and M. Posner, in *Abstracts of the Fourth International Conference on the Physics of Electronic and Atomic Collisions, Quebec*, 1965 (Science Bookcrafters, Hastings-on-Hudson, N. Y., 1965), p. 256.

[22]V. W. Hughes, R. L. Long, Jr., M. Posner, and W. Raith, in *Proceedings of the International Symposium on Electron and Photon Interactions at High Energies, Hamburg*, 1965 (Springer, Berlin, 1966), Vol. 1, p. 440.

[23]V. W. Hughes, M. S. Lubell, M. Posner and W. Raith, in *Fifth International Conference on the Physics of Electronic and Atomic Collisions, Abstracts of Papers, Leningrad*, 1967 (Nauka, Leningrad, U.S.S.R., 1967), p. 544.

[24]M. S. Lubell, V. W. Hughes, M. Posner, and W. Raith, Bull. Am. Phys. Soc. 13, 615 (1968).

[25]H. A. Tolhoek, Rev. Mod. Phys. 28, 277 (1956).

[26]U. Fano, Rev. Mod. 29, 74 (1957).

[27]P. Kusch and V. W. Hughes, *Handbuch der Physik*, edited by S. Flügge (Springer, Berlin, 1959), Vol. 37/1, p. 1.

[28]W. Raith, in *Physics of the One- and Two-Electron Atoms*, edited by F. Bopp and H. Kleinpoppen (North-Holland, Amsterdam, 1969), p. 727.

[29]A. L. Stewart, Advan. At. Mol. Phys. 3, 1 (1967).

[30]G. V. Marr and D. M. Creek, Proc. Roy. Soc. (London) A304, 233 (1968).

[31]R. D. Hudson and V. L. Carter, Phys. Rev. 139A, 1426 (1965).

[32]M. J. Seaton, Proc. Roy. Soc. (London) A208, 418 (1951).

[33]G. Baum, M. S. Lubell, and W. Raith, Phys. Rev. A (to be published).

[34]K. G. Steffen, *High Energy Beam Optics* (Interscience, New York, 1965), p. 161.

[35]J. A. Simpson, in *Methods of Experimental Physics*, edited by L. Marton, V. W. Hughes, and H. Schultz (Academic, New York, 1967), Vol. 4A, p. 84.

[36]E. Brüche and O. Scherzer, *Geometrische Elektronenoptik* (Springer, Berlin, 1934), p. 115.

[37]N. F. Mott, Proc. Roy. Soc. (London) A124, 425 (1929); A135, 429 (1932).

[38]Shin-R Lin, Phys. Rev. 133, A965 (1964).

[39]G. Holzwarth and H. J. Meister, *Tables of Asymmetry, Cross Section and Related Functions for Mott Scattering of Electrons by Screened Au and Hg Nuclei* (University of Munich, Munich, Germany, 1964); Nucl. Phys. 59, 56 (1964).

[40]W. R. Johnson, C. O. Carroll, and C. J. Mullin, Phys. Rev. 126, 352 (1962).

[41]V. A. Apalin, I. Ye. Kutikov, I. I. Lukashevich, L. A. Mikaelyan, G. V. Smirnov, and P. Ye. Spivak, Nucl. Phys. 31, 657 (1962).

[42]V. Eckardt, A. Ladage, and U. V. Moellendorff, Phys. Letters 13, 53 (1964).

[43]N. R. Lyon, *Liquid Metals Handbook*, 2nd ed. (U. S. GPO, Washington, D. C., 1952).

[44]H. C. Meyer, Jr., in *Handling and Use of the Alkali Metals* (American Chemical Soc., Washington, D. C., 1957), p. 9; E. E. Hoffman and W. D. Manly, *ibid.*, p. 82.

[45]C. E. Messer, in *The Alkali Metals* (The Chemical Society, Burlington House, London, 1967), p. 183.

[46]R. L. Christensen and D. R. Hamilton, Rev. Sci. Instr. 30, 356 (1959).

[47]A. Lemonick and F. M. Pipkin, Phys. Rev. 95, 1356 (1954).

[48]A. Lemonick, F. M. Pipkin, and D. R. Hamilton, Rev. Sci. Instr. 26, 1112 (1955).

[49]H. Lew, in *Methods of Experimental Physics*, edited by L. Marton, V. W. Hughes, and H. Schultz (Academic, New York, 1967), Vol. 4A, p. 155.

[50]E. Majorana, Nuovo Cimento 9, 43 (1932).

[51]M. J. Copley and T. E. Phipps, Phys. Rev. 48, 960 (1935).

[52]W. Schroen, Z. Physik 176, 237 (1963).

[53]*American Institute of Physics Handbook*, edited by D. E. Gray (McGraw-Hill, New York, 1963), pp. 7–14.

[54]D. L. Goldwater and W. E. Danforth, Phys. Rev. 103, 871 (1956).

[55]R. L. Long, Jr., Ph.D. thesis (Yale University, 1965) (unpublished).

[56]P. Kirkpatrick and J. G. Beckerley, Rev. Sci. Instr. 7, 24 (1936).

[57]Formvar, Type 7/95S, with a molecular weight of 16×10^3 amu, was provided by Monsanto Corp., Bircham Bend Plant, Springfield, Mass. Foils of Formvar with higher molecular weight were found to rupture during gold deposition.

[58]G. Sauerbrey, Z. Physik 155, 206 (1959).

[59]W. Eckstein, Institut für Plasmaphysik, München, Report No. IPP7/1, 1970 (unpublished); L. Mikaelyan, A. Borovoi and E. Denisov, Nucl. Phys. 47, 328 (1963); D. M. Lazarus and J. S. Greenberg, Phys. Rev. D 2, 45 (1970); J. S. Greenberg, D. P. Malone, R. L. Gluckstern, and V. W. Hughes, Phys. Rev. 120, 1393 (1960).

[60]W. Raith, R. L. Christensen, and I. Ames, in Ref. 49, p. 284.

[61]G. Glaser, Z. Naturforsch. 61, 706 (1951).

[62]M. P. Vanyukov and A. A. Mak, Usp. Fiz. Nauk 66, 301 (1958) [Sov. Phys. Usp. 1, 137 (1958)].

[63]I. S. Marshak, Usp. Fiz. Nauk 77, 229 (1962) [Sov.

Phys. Usp. 5, 478 (1962)].
[64]D. H. McMahon, A. R. Franklin, and H. R. Carleton, Rev. Sci. Instr. 37, 1142 (1966).
[65]J. F. Holzrichter and J. L. Emmett, Appl. Opt. 8, 1459 (1969).
[66]R. W. Ditchburn, Proc. Roy. Soc. (London) 117, 506 (1927).
[67]G. Herzberg, *Molecular Spectra and Molecular Structure* (Prentice-Hall, New York, 1939), p. 489.
[68]S. Dushmann, *Scientific Foundations of Vacuum Technique*, 2nd ed. (Wiley, New York, 1962), pp. 692 and 700.
[69]P. Rosenberg, Phys. Rev. 55, 1267 (1939).
[70]Y. Lee and B. H. Mahan, J. Chem. Phys. 42, 2893 (1965).
[71]R. D. Hudson and V. L. Carter, Phys. Rev. 137, A1648 (1965).
[72]M. Kasha, J. Opt. Soc. Am. 38, 929 (1948).
[73]G. Baum, M. S. Lubell, and W. Raith, Bull. Am. Phys. Soc. 16, 586 (1971).
[74]In selecting a polarized electron source for a given application, many parameters must be considered in addition to polarization P and intensity I. The celebrated figure of merit P^2I is only an aid for comparing otherwise very similar sources with regard to applications in which the statistical accuracy of asymmetry measurements is most essential.
[75]J. Berk, R. F. Koontz, and R. H. Miller, in *The Stanford Two Mile Accelerator*, edited by R. B. Neal (Benjamin, New York, 1968), Chap. 8.
[76]J. van Klinken, Nucl. Phys. 75, 161 (1966); Ph. D. thesis (University of Goningen, 1965) (unpublished).
[77]H. Steidl, E. Reichert, and H. Deichsel, Phys. Letters 17, 31 (1965).
[78]H. Deichsel and E. Reichert, Z. Physik 185, 169 (1965).
[79]K. Jost and J. Kessler, Phys. Rev. Letters 15, 575 (1965).
[80]M. Wilmers, R. Haug, and H. Deichsel, Z. Angew. Phys. 27, 204 (1969).
[81]H. Boersch, R. Schliepe, and K. E. Schriefl, Nucl. Phys. A163, 625 (1971).
[82]P. S. Farago and H. C. Siegmann, Phys. Letters 20, 279 (1966).
[83]H. Hofmann, G. Regenfus, O. Schärpf, and P. T. Kennedy, Phys. Letters 25A, 270 (1967).
[84]G. Chrobok, M. Hofmann, and G. Regenfus, Phys. Letters 26A, 551 (1968).
[85]G. Busch, M. Campagna, P. Cotti, and H. C. Siegmann, Phys. Rev. Letters 22, 597 (1969).
[86]G. Busch, M. Campagna, and H. C. Siegmann, J. Appl. Phys. 41, 1044 (1970).
[87]G. Busch, M. Campagna, and H. C. Siegmann, J. Appl. Phys. 42, 1781 (1971).
[88]U. Banninger, G. Busch, M. Campagna, and H. C. Siegmann, Phys. Rev. Letters 25, 585 (1970).
[89]G. Busch, M. Campagna, and H. C. Siegmann (unpublished).
[90]M. V. McCusker, L. L. Hatfield, and G. K. Walters, this issue, Phys. Rev. A 5, 177 (1972).
[91]U. Heinzmann, J. Kessler, and J. Lorenz, Phys. Rev. Letters 25, 1325 (1970); Z. Physik 240, 42 (1970).
[92]P. Coiffet, Compt. Rend. 264, 454 (1967).
[93]G. Baum and U. Koch, Nucl. Instr. Methods 71, 189 (1969).
[94]E. Hundhausen and H. Pauly, Z. Naturforsch. 20a, 625 (1965).
[95]Sputtering can be reduced significantly by using sealed spark lamps produced under very clean conditions, by using a low-work-function cathode material and by avoiding current oscillations [Dr. J. L. Emmett, Naval Research Laboratory, Washington, D. C. (private communication)].
[96]H. M. Brash, D. M. Campbell, P. S. Farago, A. G. A. Rae, H. C. Siegmann, and T. S. Wykes, Proc. Roy. Soc. Edinburgh A68, Pt. II, 158 (1969).
[97]M. Born and E. Wolf, *Principles of Optics*, 2nd ed. (Macmillan, New York, 1964), p. 188.

PHYSICAL REVIEW A VOLUME 5, NUMBER 1 JANUARY 1972

Combined Variable-Phase-R-Matrix Approach to Scattering Problems*

John J. Matese and Ronald J. W. Henry
Department of Physics and Astronomy, Louisiana State University, Baton Rouge, Louisiana 70803
(Received 2 August 1971)

A procedure which combines the methods of variable-phase and R-matrix theory is formulated for multichannel scattering processes. R-matrix theory is used to obtain the logarithmic derivative of the scattering functions at a radius a, beyond which all exchange potentials are negligible. Variable-phase theory is used to construct a radially dependent reaction matrix which is integrated from a to infinity. The method is applied to a two-channel model which has some of the features of the low-energy electron-hydrogen problem. Essentially exact results are obtained with as few as 40 R-matrix states (20 per channel).

I. INTRODUCTION

In recent publications,[1-3] several computational procedures have been suggested for studying low-energy electron-atom scattering which do not require the direct solution of the coupled integrodifferential equations describing the scattering process. In general, such procedures yield only approximate solutions to the coupled equations. However, the computational ease of these procedures is such as to allow for the coupling of more channels than might be attempted in a direct solution, and therefore it is hoped that any numerical inaccuracies introduced will be more than compensated